

# A CARLEMAN SEMI-DISCRETE CONVEXIFICATION METHOD COMBINED WITH DEEP LEARNING FOR ELECTRICAL IMPEDANCE TOMOGRAPHY

MICHAEL V. KLIBANOV <sup>\*</sup>, KIRILL V. GOLUBNICHY <sup>†</sup>, AND BENJAMIN JIANG<sup>‡</sup>

**Abstract.** In this paper, a new semi-discrete version of the Carleman estimate-based convexification globally convergent numerical method is developed. It is used for the delivery of the starting point for the training procedure of deep learning. An important feature of the continuous version of the convexification method is that its convergence to the true solution is independent on the availability of a good first guess about this solution. A new concept of the  $h$ -strong convexity is introduced, where  $h$  is the grid step size in the semi-discrete version of the convexification method. The  $h$ -strong convexity allows to obtain an *a priori* accuracy estimate of the starting point for the training step of the deep learning procedure. This approach is demonstrated for a highly nonlinear problem of Electrical Impedance Tomography. Results of numerical experiments for complicated media structures demonstrate the computational feasibility of this procedure.

**Key words.** coefficient inverse problems, inverse conductivity problem, global convergence, convexification Carleman estimates, deep neural networks, U-Net, computational experiments.

**AMS subject classifications.** 35R30, 65M32, 65N21, 68T07, 92C55

**1. Introduction.** We present a new concept of a two-stage numerical procedure for a broad class of Coefficient Inverse Problems (CIPs) for Partial Differential Equations (PDEs). It is well known that CIPs are highly nonlinear. On the first stage a globally convergent the so-called convexification method is applied on a coarse grid, see, e.g. [18, 19, 21, 27, 23, 25] for this method. The convexification method is based on Carleman estimates, and it is a numerical development of the initially purely theoretical idea of [4]. The publication [4] is the first one, in which the tool of Carleman estimates was introduced in the field of CIPs. The goal of [4] was to prove uniqueness and stability theorems for CIPs, see, e.g. [14, 17, 19] for some follow up publications.

The convexification method was originated in [15, 16]. The reason why the convexification is used is that conventional least squares based numerical methods for CIPs are non convex. Hence, they face the well known phenomenon of multiple local minima and ravines of corresponding cost functionals, see, e.g. [1, 2, 5, 6, 7, 8] for such functionals. In addition, we refer to [34] for a numerical example of multiple local minima. Hence, any minimization procedure for such a functional can be trapped at any local minimum. The main advantage of the convexification method is that it is free from this phenomenon.

The key point of any version of the convexification method is a construction of a weighted Tikhonov-like regularization functional  $F$ . The main feature of  $F$  is the presence of a weight function, which is the Carleman Weight Function (CWF). The CWF is used as the weight in the Carleman estimate for the corresponding PDE operator. The convergence analysis establishes then that the functional  $F$  is strongly convex on an appropriate convex bounded set  $G \subset H$  of the diameter  $d > 0$ , where  $H$  is a Hilbert space. Since restrictions on the smallness of  $d$  are not imposed, then

---

<sup>\*</sup> Department of Mathematics and Statistics, University of North Carolina at Charlotte, Charlotte, NC, 28223, USA, mklibanv@charlotte.edu,

<sup>†</sup> Department of Mathematics and Statistics, Texas Tech University, Lubbock, TX, 79409, USA, kgolubni@ttu.edu,

<sup>‡</sup> Department of Mathematical and Statistical Sciences, University of Alberta, Edmonton, AB, T6G 2J5, Canada, bjjiang@ualberta.ca

that functional is globally strongly convex. Furthermore, an accuracy estimate of the minimizer of  $F$  on the set  $G$  implies that the distance between that minimizer and the true solution of the corresponding CIP is small.

The convexification method performs slowly. Therefore, it is reasonable to use it on only the first stage of our numerical procedure, in which case a coarse grid is used. This speeds up computations quite significantly. This is certainly advantageous from the computational standpoint because of the time consuming constrained minimization procedure within the convexification method. Indeed, the same computer has required:

$$(1.1) \quad \begin{array}{l} 57 \text{ minutes of the fine grid for each image of [25]} \\ \text{and only 4 minutes on the coarse grid of this paper.} \end{array}$$

However, since only continuous versions of the convexification were considered in the past, then the use of a coarse grid causes the development of a significantly new theory: the theory of a semi-discrete version convexification method. In this case PDE operators involved in  $F$  are written in finite differences, whereas the penalty term is written in the continuous form.

The rapid solution obtained by the semi-discrete convexification method on a coarse grid is quite blurry. Hence, to improve its accuracy, we use the second stage: deep learning. More precisely, we use the solution computed by the semi-discrete version of the convexification method on the coarse grid as the starting point for the minimization of the loss function in the training procedure of deep learning. The resulting two-stage numerical procedure works quite rapidly and accurately.

Four significantly new elements of this paper are:

1. For the first time, the so-called “ $h$ -strong convexity property” is introduced. Next, this property is established for that semi-discrete analogue of the CWF-weighted Tikhonov-like objective functional, see Theorem 5.1 below. Here  $h \in (0, 1)$  is the grid step size.
2. The result of item 1 allows for estimating the accuracy of the approximation of the minimizer of the above continuous functional  $F$  by its semi-discrete analogue, see Theorems 5.2 and 5.3 below. In addition, the accuracy of the approximation of the true solution of our CIP by the semi-discrete version of the convexification method is estimated.
3. In the training procedure of deep learning the solution obtained by the semi-discrete version of the convexification method on a coarse grid is used as the starting point of iterations.
4. Therefore, items 2 and 3 result in an *a priori* accuracy estimate of the starting point of the training step of the deep learning procedure. This estimate is  $O(\sqrt{\alpha} + \sqrt{h})$ , as  $\sqrt{\alpha} + \sqrt{h} \rightarrow 0^+$ , where  $\alpha \in (0, 1)$  is a small regularization parameter used in that semi-discrete convexification method.

To our best knowledge, *a priori* accuracy estimates for starting points for the training step of deep learning were not obtained for CIPs in the past. To illustrate our concept as well as to simplify the presentation, we focus here on the CIP of Electrical Impedance Tomography (EIT) in the 2-D case, see, e.g. [3, 18] for this problem. Thus, all results below are related only to this CIP. More precisely, we focus on the recent version of the convexification method for EIT, which uses the viscosity term [25]. We refer to [11, 12, 13] for some other approaches to the issue of the global convergence for CIPs for EIT. There are many publications where deep neural network is used to EIT, see, e.g. [33].

**Remark 1.1:** *Since the convexification method is applicable to a broad class of CIPs (see, e.g. above citations), we conjecture that the approach of this paper might be extended to many other CIPs.*

A linear version of the convexification method is the Quasi-Reversibility Method (QRM), see, e.g. [17, section 2.5], [19, section 4.3], [22, 24, 26]. Unlike its nonlinear version of the convexification method, which handles highly nonlinear Coefficient Inverse Problems, the QRM is designed to solve ill-posed problems for linear PDEs. Convergence analysis of the QRM is carried out via Carleman estimates. Accuracy estimates for solutions resulting from the QRM are also a part of that analysis. provided. In particular, the solution obtained by the QRM in [22] for an ill-posed problems for the Black-Scholes equation was used in [24] as the starting point for the training step of the deep learning. Semi-discrete versions of the QRM were not studied in the past.

All functions considered below are real valued ones. The paper is organized as follows. Section 2 formulates the forward and inverse problems of EIT. In section 3 we outline the convexification method for the continuous case. In section 4 we introduce the semi-discrete version of the convexification method. In 5 we carry out convergence analysis of that semi-discrete version. In particular, we derive in 5 accuracy estimates. In section 6 we describe the deep learning procedure with *a priori* accuracy estimates on the training stage. Section 7 is devoted to numerical studies. A summary of results is presented in section 8.

**2. Statements of Forward and Inverse Problems.** Below  $\mathbf{x} = (x, y)$  denotes points in  $\mathbb{R}^2$ . We now construct such a domain  $\Omega \subset \mathbb{R}^2$ , which is convenient for our computational purpose. Let  $B, D$  be two numbers such that  $0 < B < D$ . Let  $a, b$  be two other numbers, where  $a > 0$ . Consider two concentric disks  $P_D(a, b)$  and  $P_B(a, b) \subset P_D(a, b)$  with the center at  $\mathbf{x} = (a, b)$ , and let  $E_B(a, b) = \partial P_B(a, b)$  be the circle, which is the boundary of the disk  $P_B(a, b)$ ,

$$(2.1) \quad \begin{aligned} P_D(a, b) &= \{\mathbf{x} = (x, y) : (x - a)^2 + (y - b)^2 < D^2\}, \\ P_B(a, b) &= \{\mathbf{x} = (x, y) : (x - a)^2 + (y - b)^2 < B^2\} \subset P_D(a, b), \\ E_B(a, b) &= \{\mathbf{x} = (x, y) : (x - a)^2 + (y - b)^2 = B^2\}. \end{aligned}$$

Let  $c \in (0, a)$  be a number. Define the square  $\Omega$  as

$$(2.2) \quad \Omega = \{\mathbf{x} : x \in (a - c, a + c), y \in (b - c, b + c)\}.$$

We choose  $c$  such that  $\bar{\Omega} \subset P_B(a, b)$ . Thus, in addition, by (2.2)

$$(2.3) \quad \bar{\Omega} \cap \{x = 0\} = \emptyset.$$

In our setting point sources are

$$(2.4) \quad \mathbf{x}_0 = \mathbf{x}_0(\theta) \in E_B(a, b), \theta \in [0, 2\pi].$$

We model the point sources by a smooth, compactly supported function  $g(\mathbf{x} - \mathbf{x}_0)$  which approximates the  $\delta$ -function,

$$(2.5) \quad g(\mathbf{x} - \mathbf{x}_0) = \begin{cases} C_\xi \exp\left(\frac{|\mathbf{x} - \mathbf{x}_0|^2}{|\mathbf{x} - \mathbf{x}_0|^2 - \xi^2}\right), & |\mathbf{x} - \mathbf{x}_0| < \xi, \\ 0, & |\mathbf{x} - \mathbf{x}_0| \geq \xi \end{cases}.$$

Here,  $\xi \in (0, 1)$  is a sufficiently small number such that

$$\{|\mathbf{x} - \mathbf{x}_0| < \xi\} \cap \bar{\Omega} = \emptyset, \quad \{|\mathbf{x} - \mathbf{x}_0| < \xi\} \subset P_D(a, b), \quad \forall \mathbf{x}_0 \in E_B(a, b),$$

and the number  $C_\xi$  is chosen such that

$$\int_{|\mathbf{x}-\mathbf{x}_0|<\xi} g(\mathbf{x}-\mathbf{x}_0) dx = 1, \quad \forall \mathbf{x}_0 \in E_B(a, b).$$

Let  $\sigma(\mathbf{x})$  denotes the electric conductivity coefficient. We assume that satisfies the conditions

$$(2.6) \quad \sigma \in C^2(\overline{P_D(a, b)}), \quad \sigma(\mathbf{x}) \geq 1 \text{ in } P_D(a, b),$$

$$(2.7) \quad \sigma(\mathbf{x}) = 1 \quad \text{for } \mathbf{x} \in P_B(a, b) \setminus \Omega.$$

For each  $\mathbf{x}_0 \in E_B$ , the underlying elliptic PDE is:

$$(2.8) \quad \begin{aligned} \nabla_{\mathbf{x}} \cdot (\sigma(\mathbf{x}) \nabla_{\mathbf{x}} v(\mathbf{x}, \mathbf{x}_0)) &= -g(\mathbf{x} - \mathbf{x}_0), \quad \mathbf{x} \in P_D(a, b), \\ v(\mathbf{x}, \mathbf{x}_0) &= 0, \quad \forall \mathbf{x} \in \partial P_D(a, b). \end{aligned}$$

Here  $v(\mathbf{x}, \mathbf{x}_0)$  is the voltage generated by the electric current induced at the point source  $\mathbf{x}_0 \in E_B$ . Conditions (2.2)-(2.7) imply that for every  $\gamma \in (0, 1)$  and for every  $\mathbf{x}_0 \in E_B(a, b)$  there exists unique solution  $v(\mathbf{x}, \mathbf{x}_0) \in C^{3+\gamma}(\overline{P_D(a, b)})$  of problem (2.8). Here  $C^{3+\gamma}(\overline{P_D(a, b)})$  is the Hölder space [9]. By the maximum principle [9], there exists a number  $\beta > 0$  such that  $v(\mathbf{x}, \mathbf{x}_0) \geq \beta$ ,  $\forall \mathbf{x} \in \overline{\Omega}$ ,  $\forall \mathbf{x}_0 \in E_B(a, b)$ .

Let  $\Gamma_0 \subset \partial\Omega$  be the right side of the square  $\Omega$  in (2.2),

$$(2.9) \quad \Gamma_0 = \{\mathbf{x} = (x, y) : x = a + c, y \in (b - c, b + c)\},$$

We formulate the coefficient inverse problem as follows:

**Coefficient Inverse Problem (CIP).** For each  $\mathbf{x}_0 \in E_B(a, b)$  let  $v(\mathbf{x}, \mathbf{x}_0) \in C^{3+\alpha}(\overline{P_D(a, b)})$  be the above solution of problem (2.8). Assume that the following functions  $h_0(\mathbf{x}, \mathbf{x}_0)$  and  $h_1(\mathbf{x}, \mathbf{x}_0)$  are given:

$$(2.10) \quad \begin{aligned} v(\mathbf{x}, \mathbf{x}_0) &= h_0(\mathbf{x}, \mathbf{x}_0), \quad \forall \mathbf{x} \in \partial\Omega, \\ v_x(\mathbf{x}, \mathbf{x}_0) &= h_1(\mathbf{x}, \mathbf{x}_0), \quad \forall \mathbf{x} \in \Gamma_0, \\ &\quad \forall \mathbf{x}_0 \in E_B(a, b). \end{aligned}$$

Find the coefficient  $\sigma(\mathbf{x})$  in for  $\mathbf{x} \in \Omega$ .

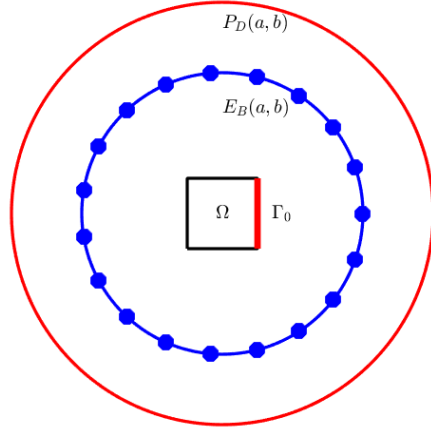


FIG. 1. A schematic diagram of our measurements. The large disk is the domain  $P_D(a, b)$  where the forward problem is solved. The smaller circle is the circle  $E_B(a, b)$  where point sources are located. The square is our domain of interest  $\Omega$ , where the CIP is solved.

As to the above CIP, two versions of the convexification method for it were published in [18, 25]. Below we follow the version of [25]. First, the convexification method, transforms the inverse problem in a system of two coupled elliptic PDEs with a viscosity term, subject to the Cauchy boundary conditions. These PDEs do not contain the unknown coefficient  $\sigma(\mathbf{x})$ . Within the framework of the convexification method, a viscosity term was introduced for the first time in [20] for the numerical solution of the Hamilton-Jacobi equation. We also refer to [29] in this regard. In both [25] and the current paper, an extended idea of [20, 29] about the viscosity term in the convexification method is used. The presence of the viscosity term enables us to avoid the truncation of a certain Fourier-like series, such as the one in [18]. In addition, the viscosity term was used in the convexification method for CIPs in [23, 26].

**3. The Carleman Estimate-Based Convexification Method for Coefficient Inverse Problem (2.8)-(2.10).** For a better understanding of the convexification related material of this paper, we outline in this section the continuous version of this method, which we take from [25].

**3.1. Transformation procedure.** First, we change variables as  $V(\mathbf{x}, \mathbf{x}_0) = \sqrt{\sigma(\mathbf{x})}v(\mathbf{x}, \mathbf{x}_0)$ . Using (2.8) and (2.10) we obtain

$$(3.1) \quad \Delta V + r(\mathbf{x})V = 0, \text{ in } \Omega,$$

$$(3.2) \quad \begin{aligned} V(\mathbf{x}, \mathbf{x}_0) &= h_0(\mathbf{x}, \mathbf{x}_0), \quad \mathbf{x} \in \partial\Omega, \\ V_x(\mathbf{x}, \mathbf{x}_0) &= h_1(\mathbf{x}, \mathbf{x}_0), \quad \forall \mathbf{x} = (a+c, y) \in \Gamma_0, \quad y \in (b-c, b+c), \\ &\quad \forall \mathbf{x}_0 \in E_B(a, b), \end{aligned}$$

$$(3.3) \quad r(\mathbf{x}) = \frac{\Delta(\sqrt{\sigma(\mathbf{x})})}{\sqrt{\sigma(\mathbf{x})}}.$$

Let  $\mathbf{x}_0 = \mathbf{x}_0(\theta)$ , where the angle  $\theta \in [0, 2\pi]$ . Next, we set

$$(3.4) \quad \psi(\mathbf{x}, \theta) = \ln V(\mathbf{x}, \theta)$$

and substitute this in (2.10). We obtain

$$(3.5) \quad \Delta\psi + (\nabla\psi)^2 + r(\mathbf{x}) = 0, \quad \mathbf{x} \in \Omega.$$

Note that a logarithmic transformation for a CIP was first used in [15, the next line after (1.14)]. Recalling (2.4) and differentiating (3.5) with respect to  $\theta$  we eliminate the unknown coefficient  $r(x)$ . If the function  $\psi(x, \theta)$  is found, then by (3.5)

$$(3.6) \quad r(\mathbf{x}) = -\frac{1}{2\pi} \int_0^{2\pi} (\Delta\psi + (\nabla\psi)^2)(\mathbf{x}, \theta) d\theta, \quad x \in \Omega.$$

Given  $r(x)$ , the question of finding the target coefficient  $\sigma(\mathbf{x})$  is addressed below.

The above differentiation with respect to  $\theta$  leads to:

$$(3.7) \quad \Delta\psi_\theta + 2\nabla\psi_\theta\nabla\psi = 0, \quad x \in \Omega.$$

However, (3.7) is one equation with two unknown functions  $\psi$  and  $\psi_\theta$ . To express  $\psi$  via  $\psi_\theta$ , one might try to use

$$\psi(\mathbf{x}, \theta) = \int_{\theta_0}^{\theta} \psi_\theta(\mathbf{x}, s) ds + \psi(\mathbf{x}, \theta_0)$$

for a certain  $\theta_0 \in (0, 2\pi)$ . However, the function  $\psi(\mathbf{x}, \theta_0)$  is unknown for any value of  $\theta_0$ . This causes the introduction of a viscosity term  $-\varepsilon\Delta\psi$  with a small parameter  $\varepsilon \in (0, 1)$  [25]. This term complements (3.7) with the following equation

$$(3.8) \quad -\varepsilon\Delta\psi + \Delta\psi_\theta + 2\nabla\psi_\theta\nabla\psi = 0, \quad \mathbf{x} \in \Omega.$$

Denote

$$(3.9) \quad \phi = \psi_\theta - \varepsilon\psi.$$

Then (3.7) and (3.8) lead to the following system of coupled nonlinear PDEs for the functions  $\psi_\theta$  and  $\phi$ ,

$$(3.10) \quad F_1(\psi_\theta, \phi)(\theta) = \Delta\psi_\theta + 2\nabla\psi_\theta\nabla\left(\frac{\psi_\theta - \phi}{\varepsilon}\right) = 0, \quad \mathbf{x} \in \Omega, \quad \theta \in [0, 2\pi],$$

$$(3.11) \quad F_2(\psi_\theta, \phi)(\theta) = \Delta\phi + 2\nabla\psi_\theta\nabla\left(\frac{\psi_\theta - \phi}{\varepsilon}\right) = 0, \quad \mathbf{x} \in \Omega, \quad \theta \in [0, 2\pi].$$

This system is subject to the overdetermined boundary conditions derived from the data (3.2)

$$(3.12) \quad \psi_\theta(\mathbf{x}, \theta) |_{\mathbf{x} \in \partial\Omega} = \partial_\theta s_0(\mathbf{x}, \theta), \quad (\mathbf{x}, \theta) \in \partial\Omega \times [0, 2\pi],$$

$$(3.13) \quad \partial_x(\partial_\theta\psi(\mathbf{x}, \theta)) |_{\mathbf{x} \in \Gamma_0} = \partial_\theta s_1(\mathbf{x}, \theta), \quad \forall (\mathbf{x}, \theta) \in \Gamma_0 \times [0, 2\pi],$$

$$(3.14) \quad \phi(\mathbf{x}, \theta) |_{\mathbf{x} \in \partial\Omega} = \partial_\theta s_0(\mathbf{x}, \theta) - \varepsilon s_0(\mathbf{x}, \theta), \quad \forall (\mathbf{x}, \theta) \in \partial\Omega \times [0, 2\pi],$$

$$(3.15) \quad \partial_x \phi(\mathbf{x}, \theta) = \partial_\theta s_1(\mathbf{x}, \theta) - \varepsilon s_1(\mathbf{x}, \theta), \quad \forall (\mathbf{x}, \theta) \in \Gamma_0 \times [0, 2\pi].$$

where  $s_0$  and  $s_1$  are derived from the data  $h_0$  and  $h_1$  (see equations (3.9) and (3.10) in [25]). Introduce a new notation for convenience

$$(3.16) \quad (q, p)(\mathbf{x}, \theta) = (\psi_\theta, \phi)(\mathbf{x}, \theta).$$

The transformation procedure is complete.

**3.2. The Carleman estimate.** The construction of the globally convergent convexification method for our CIP is based on a Carleman estimate [25]. Denote

$$(3.17) \quad H_0^2(\Omega) = \{u \in H^2(\Omega) : u|_{\partial\Omega} = 0, \partial_x u|_{\Gamma_0} = 0\}.$$

Having (2.2) and (2.9), we define Carleman Weight Function (CWF) as

$$(3.18) \quad W_\kappa(\mathbf{x}) = \exp(2\kappa x^2),$$

where  $\kappa \geq 1$  is a parameter.

**Theorem 3.1** (Carleman estimate [19, Theorem 10.3.1]). *There exists a sufficiently large number  $\kappa_0 = \kappa_0(\Omega) \geq 1$  and a number  $C = C(\Omega) > 0$ , both numbers depending only on  $\Omega$ , such that with the CWF  $W_\kappa(\mathbf{x})$  as in (3.18) the following Carleman estimate holds:*

$$\begin{aligned} \int_{\Omega} (\Delta u)^2 W_\kappa(\mathbf{x}) d\mathbf{x} &\geq \frac{C}{\kappa} \int_{\Omega} (u_{xx}^2 + u_{xy}^2 + u_{yy}^2) W_\kappa(\mathbf{x}) d\mathbf{x} + \\ &+ C\kappa \int_{\Omega} (\nabla u)^2 W_\kappa(\mathbf{x}) d\mathbf{x} + C\kappa^3 \int_{\Omega} u^2 W_\kappa(\mathbf{x}) d\mathbf{x}, \\ &\forall \kappa \geq \kappa_0, \forall u \in H_0^2(\Omega). \end{aligned}$$

Everywhere below  $C = C(\Omega) > 0$  denotes different numbers depending only on the domain  $\Omega$ . We note that there is another CWF for a general elliptic operator of the second order, see, e.g. [19, section 2.4], [28, §1 of Chapter 4]. However, that CWF depends on two large parameters instead of one in (3.18). The latter makes it hard to use that CWF for computations.

**3.3. The globally strongly convex CWF-weighted Tikhonov-like functional.** The CWF (3.18) is the weight function for our CWF-weighted Tikhonov-like cost functional. We point out that even though  $\kappa$  is required to be sufficiently large, our rich computational experience of working with the convexification method (see the above citations) shows that actually  $\kappa \in [1, 5]$  is sufficient. In this regard, there is a similarity here to an asymptotic theory. Indeed, typically such a theory states that if a parameter  $X$  is sufficiently large, then a certain formula  $Y$  is sufficiently accurate. However, in any specific computational practice only numerical studies can establish which exactly values of  $Y$  ensure a good accuracy of the formula  $Y$ .

Similarly with (3.17) we define the space  $H_0^6(\Omega)$  as

$$(3.19) \quad H_0^6(\Omega) = \{u \in H^6(\Omega) : u|_{\partial\Omega} = 0, \partial_x u|_{\Gamma_0} = 0\}.$$

Define spaces  $H_{1,\theta}$  and  $H_{1,2,\theta}$  depending on the parameter  $\theta \in [0, 2\pi]$ ,

$$(3.20) \quad H_{1,\theta} = \left\{ \begin{array}{l} q(\mathbf{x}, \theta) : q(\mathbf{x}, \theta) \in H^6(\Omega), \\ \|q(\mathbf{x}, \theta)\|_{H_{1,\theta}}^2 = \|q(\mathbf{x}, \theta)\|_{H^6(\Omega)}^2 < \infty, \forall \theta \in [0, 2\pi], \end{array} \right\},$$

$$H_{1,\theta}^0 = \{q(\mathbf{x}, \theta) : q(\mathbf{x}, \theta) \in H_0^6(\Omega)\},$$

$$H_{1,2,\theta} = H_{1,\theta} \times H_{1,\theta}, \quad H_{1,2,\theta}^0 = H_{1,\theta}^0 \times H_{1,\theta}^0,$$

$$\|(q, p)(\mathbf{x}, \theta)\|_{H_{1,2,\theta}}^2 = \|q(\mathbf{x}, \theta)\|_{H_{1,\theta}}^2 + \|p(\mathbf{x}, \theta)\|_{H_{1,\theta}}^2.$$

We note that while in [25, formula (4.1)] the norm  $\|q(x, \theta)\|_{H^3(\Omega)}$  was used in the direct analog of (3.20), here we use the norm  $\|q(x, \theta)\|_{H^6(\Omega)}$ . This is because of the finite difference approximations of the second order derivatives with the  $O(h^2)$ -accuracy, which we use below in the discrete version of the convexification. Indeed, by Sobolev embedding theorem

$$(3.21) \quad \begin{aligned} (q, p)(\mathbf{x}, \theta) &\in C^4(\overline{\Omega}) \times C^4(\overline{\Omega}), \quad \forall (q, p)(\mathbf{x}, \theta) \in H_{1,2,\theta}, \\ \|(q, p)(\mathbf{x}, \theta)\|_{C^4(\overline{\Omega}) \times C^4(\overline{\Omega})} &\leq C \|(q, p)(\mathbf{x}, \theta)\|_{H_{1,2,\theta}}, \\ \forall (q, p)(\mathbf{x}, \theta) &\in H_{1,2,\theta}, \quad \forall \theta \in [0, 2\pi]. \end{aligned}$$

**Remark 3.1.** *Regarding to the smoothness conditions in (3.19)-(3.21), we note that, as a rule, extra smoothness requirements are not considered as serious restrictions in the theory of CIPs, see, e.g. [30, 31].*

Let  $A > 0$  be an arbitrary number, which we fix. Using notation (3.16), we define the set  $G_\theta(A) \subset H_{1,2,\theta}$  as:

$$(3.22) \quad G_\theta(A) = \left\{ \begin{array}{l} (q, p)(\mathbf{x}, \theta) \in H_{1,2,\theta} : \|(q, p)(\mathbf{x}, \theta)\|_{H_{1,2,\theta}} < A, \\ q \text{ satisfies boundary conditions (3.12), (3.13),} \\ p \text{ satisfies boundary conditions (3.14), (3.15),} \\ \forall \theta \in [0, 2\pi] \end{array} \right\}.$$

Hence, by (3.21) and (3.22)

$$(3.23) \quad \|(q, p)(\mathbf{x}, \theta)\|_{C^4(\overline{\Omega}) \times C^4(\overline{\Omega})} \leq CA, \quad \forall (q, p)(\mathbf{x}, \theta) \in H_{1,2,\theta}, \quad \forall \theta \in [0, 2\pi].$$

We define the functional

$$J_{\kappa,\alpha} : \overline{G_\theta(A)} \rightarrow \mathbb{R}, \quad \forall \theta \in [0, 2\pi]$$

as (see equations (4.1) and (4.2) in [25])

$$(3.24) \quad \begin{aligned} J_{\kappa,\alpha}(q, p)(\theta) &= \sqrt{\varepsilon} \int_{\Omega} \left[ (F_1(q, p)(\mathbf{x}, \theta))^2 + (F_2(q, p)(\mathbf{x}, \theta))^2 \right] W_\kappa(\mathbf{x}) \, d\mathbf{x} + \\ &+ \alpha \|(q, p)(\mathbf{x}, \theta)\|_{H^6(\Omega) \times H^6(\Omega)}^2, \quad \forall \theta \in [0, 2\pi], \end{aligned}$$

where  $\alpha \in (0, 1)$  is the regularization parameter. We consider the following minimization problem:

**Minimization Problem.** Minimize the functional  $J_{\kappa,\alpha}(q, p)(\theta)$  on the set  $\overline{G_\theta(A)}$  for each  $\theta \in [0, 2\pi]$ .

**Theorem 3.2** (global strong convexity) [25]. *The following hold true:*

1. For each  $\kappa > 0$ , for each  $\theta \in [0, 2\pi]$  and for each pair  $(q, p) \in \overline{G_\theta(A)}$  the functional  $J_{\kappa, \alpha}(q, p)(\theta)$  has the Fréchet derivative

$$(3.25) \quad J'_{\kappa, \alpha}(q, p)(\theta) \in H^0_{1,2,\theta}, \quad \forall \theta \in [0, 2\pi].$$

2. Let  $\kappa_0 = \kappa_0(\Omega) \geq 1$  be the number of Theorem 3.1. There exists a sufficiently large number  $\kappa_1 = \kappa_1(A, \Omega, \varepsilon) \geq \kappa_0$  such that for each  $\kappa \geq \kappa_1$  the functional  $J_{\kappa, \alpha}(q, p)$  is strongly convex on the set  $\overline{G_\theta(A)}$ , i.e. there exists a number  $C_1 = C_1(A, \Omega, \varepsilon) > 0$  such that

$$(3.26) \quad \begin{aligned} & J_{\kappa, \alpha}(q_2, p_2)(\theta) - J_{\kappa, \alpha}(q_1, p_1)(\theta) - J'_{\kappa, \alpha}(q_1, p_1)(\theta)(q_2 - q_1, p_2 - p_1)(\mathbf{x}, \theta) \geq \\ & \geq C_1 \exp\left(2\kappa(a - c_1)^2\right) \|(q_2 - q_1, p_2 - p_1)(\mathbf{x}, \theta)\|_{H^2(\Omega) \times H^2(\Omega)}^2 + \\ & \quad + \alpha \|(q_2 - q_1, p_2 - p_1)(\mathbf{x}, \theta)\|_{H_{1,2,\theta}}^2, \\ & \quad \forall \theta \in [0, 2\pi], \quad \forall (q_1, p_1)(\mathbf{x}, \theta), (q_2, p_2)(\mathbf{x}, \theta) \in \overline{G_\theta(A)}, \quad \forall \kappa \geq \kappa_1. \end{aligned}$$

Numbers  $\kappa_1(A, \Omega, \varepsilon)$  and  $C_1(A, \Omega, \varepsilon)$  depend only on listed parameters.

3. For every  $\kappa \geq \kappa_1$  and for every  $\theta \in [0, 2\pi]$  there exists unique minimizer  $(q_{\min, \kappa, \alpha}, p_{\min, \kappa, \alpha})(\mathbf{x}, \theta) \in \overline{G_\theta(A)}$  of the functional  $J_{\kappa, \alpha}(q, p)(\theta)$  on the set  $\overline{G_\theta(A)}$ . In addition,

$$(3.27) \quad \begin{aligned} & J'_{\kappa, \alpha}(q_{\min, \kappa, \alpha}, p_{\min, \kappa, \alpha})(\theta)((q_{\min, \kappa, \alpha} - q, p_{\min, \kappa, \alpha} - p)(\mathbf{x}, \theta)) \leq 0, \\ & \quad \forall \theta \in [0, 2\pi], \quad \forall (q, p)(\mathbf{x}, \theta) \in \overline{G_\theta(A)}. \end{aligned}$$

Everywhere below  $C_1 = C(A, \Omega, \varepsilon) > 0$  denotes different numbers depending only on listed parameters. Suppose now that the minimizer  $(q_{\min, \kappa, \alpha}, p_{\min, \kappa, \alpha})(\mathbf{x}, \theta)$  of the functional  $J_{\kappa, \alpha}(q, p)(\theta)$  on the set  $\overline{G_\theta(A)}$  is found. Next, keeping in mind (3.6), (3.9) and (3.16), we set

$$(3.28) \quad \partial_\theta \psi_{\min, \kappa, \alpha}(\mathbf{x}, \theta) = q_{\min, \kappa, \alpha}(\mathbf{x}, \theta), \quad \phi_{\min, \kappa, \alpha}(\mathbf{x}, \theta) = p_{\min, \kappa, \alpha}(\mathbf{x}, \theta),$$

$$(3.29) \quad \psi_{\min, \kappa, \alpha}(\mathbf{x}, \theta) = \frac{\partial_\theta \psi_{\min, \kappa, \alpha}(\mathbf{x}, \theta) - \phi_{\min, \kappa, \alpha}(\mathbf{x}, \theta)}{\varepsilon},$$

$$(3.30) \quad r_{\kappa, \alpha}(\mathbf{x}) = -\frac{1}{2\pi} \int_0^{2\pi} \left( \Delta \psi_{\min, \kappa, \alpha} + (\nabla \psi_{\min, \kappa, \alpha})^2 \right)(\mathbf{x}, \theta) d\theta, \quad \mathbf{x} \in \Omega.$$

Denote

$$(3.31) \quad w(\mathbf{x}) = \sqrt{\sigma(\mathbf{x})}.$$

By (3.3) we now need to solve the following elliptic equation:

$$(3.32) \quad \Delta w - r_{\kappa,\alpha}(\mathbf{x}) w = 0, \quad \mathbf{x} \in \Omega.$$

It follows from (2.6), (2.7) and (3.31) that this equation should be complemented by two boundary conditions

$$(3.33) \quad w|_{\partial\Omega} = 1, \quad \partial_\nu w|_{\partial\Omega} = 0,$$

where  $\partial_\nu$  is the normal derivative at  $\partial\Omega$ . Next, we assign the reconstructed function  $\sigma_{\kappa,\alpha}(\mathbf{x})$  as:

$$(3.34) \quad \sigma_{\kappa,\alpha}(\mathbf{x}) = w^2(\mathbf{x}).$$

Problem (3.32), (3.33) has an overdetermination in the boundary conditions. Hence, this problem was solved in [25] by the Quasi-Reversibility Method, which was mentioned in section 1. More precisely, the following functional  $I(w)$  was minimized in [25] on the set of functions  $w \in H^2(\Omega)$  satisfying boundary conditions (3.33)

$$(3.35) \quad I(w) = \int_{\Omega} (\Delta w - r_{\kappa,\alpha}(\mathbf{x}) w)^2 d\mathbf{x}.$$

**3.4. The accuracy of the minimizer.** The minimizer  $(q_{\min,\kappa,\alpha}, p_{\min,\kappa,\alpha})(\mathbf{x}, \theta)$  of the functional  $J_{\kappa,\alpha}(q, p)(\theta)$  is called “regularized solution” in the theory of Ill-Posed Problems [35]. Following one of conventional postulates of this theory, we assume the existence of the true solution  $\sigma^*(\mathbf{x})$  of our CIP satisfying conditions (2.6), (2.7) with the noiseless data  $h_0^*(\mathbf{x}, \theta), h_1^*(\mathbf{x}, \theta)$  in (2.10). An important question is the question of an estimate of the accuracy of the regularized solution, i.e. an estimate of a norm of the difference between  $(q_{\min,\kappa,\alpha}, p_{\min,\kappa,\alpha})(\mathbf{x}, \theta)$  and  $(q^*, p^*)(\mathbf{x}, \theta)$ , where the last pair corresponds to  $\sigma^*(\mathbf{x})$ . As it follows from the discussion of the previous section, below Theorem 3.2, this estimate, in turn leads to an estimate of a certain norm of the difference  $\sigma_{\kappa,\alpha}(\mathbf{x}) - \sigma^*(\mathbf{x})$ . Such an estimate was derived in [25, Theorem 5.3]. To simplify the presentation, that estimate was derived in [25, Theorem 5.3] for a norm of the difference  $r_{\kappa,\alpha}(\mathbf{x}) - r^*(\mathbf{x})$ , where  $r^*(\mathbf{x})$  is generated by  $\sigma^*(\mathbf{x})$  as in (3.3).

While the case of noisy data was considered in [25, Theorem 5.3], we simplify the presentation here by assuming that our data (2.10) are noiseless. This is because we only outline here the results of [25] without going to some details. Thus, we estimate here the difference  $r_{\kappa,\alpha}(\mathbf{x}) - r^*(\mathbf{x})$ , assuming that

$$(3.36) \quad h_0(\mathbf{x}, \theta) = h_0^*(\mathbf{x}, \theta), \quad h_1(\mathbf{x}, \theta) = h_1^*(\mathbf{x}, \theta).$$

Since we now work in the framework of the viscosity solution, then, based on (3.7), (3.8) and (3.16), we assume that the pair  $(q^*, p^*)(\mathbf{x}, \theta) = (\psi_\theta^*, \phi^*)(\mathbf{x}, \theta)$  satisfies equations (3.10) and (3.11), i.e.

$$(3.37) \quad F_1(q^*, p^*)(\mathbf{x}, \theta) = F_2(q^*, p^*)(\mathbf{x}, \theta) = 0, \quad \forall \mathbf{x} \in \Omega, \quad \forall \theta \in [0, 2\pi].$$

**Theorem 3.3:**

1. Let the function  $\sigma^*(\mathbf{x})$  be the exact solution of our CIP satisfying conditions (2.6), (2.7) and with the noiseless data  $h_0^*(\mathbf{x}, \theta), h_1^*(\mathbf{x}, \theta)$ . Assume that we have noiseless data in (2.10), i.e. assume that (3.36) holds.

2. Also, let the function  $r^*(\mathbf{x})$  be linked with the function  $\sigma^*(\mathbf{x})$  via the direct analog of formula (3.3). Let  $(q^*, p^*)(\mathbf{x}, \theta)$  be the pair of functions generated by the function  $\sigma^*(\mathbf{x})$ . Let  $G_\theta(A)$  be the set of vector functions defined in (3.22). Assume that

$$(3.38) \quad (q^*, p^*)(\mathbf{x}, \theta) \in G_\theta(A).$$

3. Let  $\kappa_1$  be the number of Theorem 3.2 and let  $\kappa \geq \kappa_1$ . Let  $(q_{\min, \kappa, \alpha}, p_{\min, \kappa, \alpha})(\mathbf{x}, \theta) \in G_\theta(A)$  be the minimizer of the functional  $J_{\kappa, \alpha}(q, p)(\theta)$  on the set  $G_\theta(A)$ , which was found in Theorem 3.2. Let the function  $r_{\kappa, \alpha}(x)$  being found via (3.28)-(3.30) be the corresponding approximation for function  $r^*(\mathbf{x})$ . Then the following accuracy estimates are valid:

$$(3.39) \quad \begin{aligned} & \| (q_{\min, \kappa, \alpha} - q^*)(\mathbf{x}, \theta) \|_{H^2(\Omega)} + \| (p_{\min, \kappa, \alpha} - p^*)(\mathbf{x}, \theta) \|_{H^2(\Omega)} \leq \\ & \leq C_1 \sqrt{\alpha} \exp \left[ -\kappa (a - c)^2 \right], \quad \forall \theta \in [0, 2\pi], \end{aligned}$$

$$(3.40) \quad \| r_{\kappa, \alpha} - r^* \|_{L_2(\Omega)} \leq C_1 \sqrt{\alpha} \exp \left[ -\kappa (a - c)^2 \right].$$

**Proof.** We provide this proof here since it is different from the one of [25, Theorem 5.3]. Recall (3.16). The functional  $J_{\kappa, \alpha}(q, p)(\theta)$  in (3.24) is the sum of two parts. The first part contains differential operators  $F_1(q, p)(\theta)$  and  $F_2(q, p)(\theta)$  in (3.10) and (3.11), which are generated by our CIP. And the second part contains only the regularization term  $\alpha \| (q, p)(\mathbf{x}, \theta) \|_{H_{1,2,\theta}}^2$ , which is not directly linked to our CIP. For each  $\theta \in [0, 2\pi]$  this can be written as:

$$(3.41) \quad J_{1, \kappa, \alpha}(q, p)(\theta) = \sqrt{\varepsilon} \int_{\Omega} \left[ (F_1(q, p)(\mathbf{x}, \theta))^2 + (F_2(q, p)(\mathbf{x}, \theta))^2 \right] W_\kappa(\mathbf{x}) d\mathbf{x},$$

$$(3.42) \quad J_{2, \kappa, \alpha}(q, p)(\theta) = \alpha \| (q, p)(\mathbf{x}, \theta) \|_{H_{1,2,\theta}}^2,$$

$$(3.43) \quad J_{\kappa, \alpha}(q, p)(\theta) = J_{1, \kappa, \alpha}(q, p)(\theta) + J_{2, \kappa, \alpha}(q, p)(\theta).$$

By (3.20), (3.22), (3.37), (3.38) and (3.41)-(3.43)

$$(3.44) \quad J_{\kappa, \alpha}(q^*, p^*)(\theta) = \alpha \| (q^*, p^*)(\mathbf{x}, \theta) \|_{H^6(\Omega) \times H^6(\Omega)}^2 \leq \alpha A, \quad \forall \theta \in [0, 2\pi].$$

Next, by (3.26)

$$(3.45) \quad \begin{aligned} & J_{\kappa, \alpha}(q^*, p^*)(\theta) - J_{\kappa, \alpha}(q_{\min, \kappa, \alpha}, p_{\min, \kappa, \alpha})(\theta) - \\ & - J'_{\kappa, \alpha}((q_{\min, \kappa, \alpha}, p_{\min, \kappa, \alpha}))(\theta) ((q^* - q_{\min, \kappa, \alpha}, p^* - p_{\min, \kappa, \alpha})(\mathbf{x}, \theta)) \geq \\ & \geq C_1 \exp \left( 2\kappa (a - c)^2 \right) \| (q^* - q_{\min, \kappa, \alpha}, p^* - p_{\min, \kappa, \alpha})(\mathbf{x}, \theta) \|_{H^2(\Omega) \times H^2(\Omega)}^2, \end{aligned}$$

$$\forall \theta \in [0, 2\pi].$$

Using (3.27), we obtain

$$(3.46) \quad -J'_{\kappa, \alpha}((q_{\min, \kappa, \alpha}, p_{\min, \kappa, \alpha}))(\theta)(q^* - q_{\min, \kappa, \alpha}, p^* - p_{\min, \kappa, \alpha})(\mathbf{x}, \theta) \leq 0.$$

In addition,

$$(3.47) \quad -J_{\kappa, \alpha}((q_{\min, \kappa, \alpha}, p_{\min, \kappa, \alpha}))(\theta) \leq 0.$$

Hence, using (3.44)-(3.47), we obtain

$$\|(q^* - q_{\min, \kappa, \alpha}, p^* - p_{\min, \kappa, \alpha})(\mathbf{x}, \theta)\|_{H^2(\Omega) \times H^2(\Omega)}^2 \leq C_1 \alpha \exp\left(-2\kappa(a-c)^2\right),$$

which implies the first target accuracy estimate (3.39). The second target accuracy estimate (3.40) follows from (3.6), (3.9), (3.16), (3.30) and (3.39).  $\square$

**4. The Semi-Discrete Analogue of the Functional  $J_{\kappa, \alpha}$ .** We call the case of this section “semi-discrete” because we consider a discrete analog of the functional  $J_{1, \kappa, \alpha}(q, p)(\theta)$  in (3.41), whereas we consider the functional  $J_{2, \kappa, \alpha}(q, p)(\theta)$  in (3.42) in its original continuous form. We need the material of this section since we apply the convexification method on a coarse grid on the first stage of our numerical procedure: due to a slow performance of this method on a fine grid.

**4.1. Discretization.** Recall definition (2.2) of the domain  $\Omega$  and consider the following grid  $\{(x_i, y_j)\}_{i, j=0}^{n+1} \subset \bar{\Omega}$  in  $\bar{\Omega}$  with the grid step size  $h \in (0, 1)$  and  $n > 4$

$$(4.1) \quad \begin{aligned} a - c = x_0 < x_1 < \dots < x_n < x_{n+1} = a + c, & \quad x_i - x_{i-1} = h, \\ b - c = y_0 < y_1 < \dots < y_n < y_{n+1} = b + c, & \quad y_j - y_{j-1} = h. \end{aligned}$$

Everywhere below  $O(h^k)$  denotes different functions such that

$$(4.2) \quad |O(h^k)| \leq C_1 h^k, k > 0.$$

Recall that  $\Gamma_0 \subset \partial\Omega$  was defined in (2.9). Denote

$$(4.3) \quad \begin{aligned} \Omega^h &= \{(x_i, y_j)\}_{i, j=1}^n, \\ \bar{\Omega}^h &= \{(x_i, y_j)\}_{i, j=0}^{n+1}, \\ \partial\Omega^h &= \bar{\Omega}^h \setminus \Omega^h, \\ \Gamma_0^h &= \{(a + c, y_j), j = 0, \dots, n + 1\}. \end{aligned}$$

Denote the running point in  $\bar{\Omega}^h$  as  $\mathbf{x}_{i, j}^h = (x_i, y_j)$ ,  $\forall i, j = 0, \dots, n + 1$ . Any function  $z(\mathbf{x}) \in C(\bar{\Omega})$  generates the discrete function  $z^h(\mathbf{x}_{i, j}^h)$  defined on the grid (4.1). Hence,

$$(4.4) \quad z^h(\mathbf{x}_{i, j}^h) = z(x_i, y_j), i, j = 0, \dots, n + 1.$$

Let the function  $f(\mathbf{x}) \in C^4(\bar{\Omega})$ . We define its first derivative with respect to  $x$  in finite differences at the points  $(x_i, y_j) \in \Omega^h$ ,  $i, j = 1, \dots, n$  as:

$$(4.5) \quad \partial_x^h f_{i, j} = \partial_x^h f^h(x_i, y_j) = \frac{f(x_{i+1}, y_j) - f(x_{i-1}, y_j)}{2h}.$$

Next, its second derivative with respect to  $x$  in finite differences at the points  $(x_i, y_j) \in \Omega^h$ ,  $i, j = 1, \dots, n$  is defined as:

$$(4.6) \quad \partial_x^{h,2} f_{i,j} = \partial_x^{h,2} f^h(x_i, y_j) = \frac{f(x_{i+1}, y_j) - 2f(x_i, y_j) + f(x_{i-1}, y_j)}{h^2}.$$

In addition, because of the Neumann boundary conditions (3.13) and (3.15) at  $\Gamma_0$ , we define its finite difference approximation at points  $f(x_{n+1}, y_k) = f(a+c, y_k)$  as:

$$(4.7) \quad \begin{aligned} & \partial_x^h f_{n+1,j} = \partial_x^h f^h(a+c, y_j) = \\ & = [3f(a+c, y_j) - 4f(x_n, y_j) + f(x_{n-1}, y_j)] / (2h), \\ & (a+c, y_j) \in \Gamma_0^h, \quad j = 0, \dots, n+1. \end{aligned}$$

Note that

$$(4.8) \quad \begin{aligned} & \partial_x^h f_{i,j}^h = f_x(x_i, y_j) + O(h^2), \quad \partial_x^{h,2} f_{i,j}^h = f_{xx}(x_i, y_j) + O(h^2), \\ & \quad \quad \quad i, j = 1, \dots, n, \\ & \partial_x^h f_{n+1,k} = \partial_x^h f^h(a+c, y_k) = f_x(a+c, y_k) + O(h^2), \quad k = 0, \dots, n+1, \\ & \quad \quad \quad |O(h^2)| \leq C \|f\|_{C^4(\bar{\Omega})} h^2, \\ & \quad \quad \quad \forall f \in C^4(\bar{\Omega}). \end{aligned}$$

First and second finite difference derivatives  $\partial_x f_{i,j}^h$  and  $\partial_y^2 f_{i,j}^h$  with respect to  $y$  as well as the mixed derivative  $\partial_{xy}^{h,2} f_{i,j}^h$  at the points  $(x_i, y_j) \in \Omega^h$  are defined similarly, and analogs of formulas (4.8) hold. Next, we consider finite difference analogs of the Laplace operator and the gradient vector,

$$(4.9) \quad \Delta^h f_{i,j} = \partial_x^{h,2} f_{i,j} + \partial_y^{h,2} f_{i,j}, \quad \nabla^h f_{i,j} = (\partial_x^h f_{i,j}, \partial_y^h f_{i,j}).$$

Given the above constructions, Proposition 3.1 follows immediately from (4.4)-(4.9) and Taylor formula.

**Proposition 4.1.** *For each function  $f \in C^4(\bar{\Omega})$  the following accuracy estimates are valid for points  $\mathbf{x}_{i,j}^h \in \Omega^h$  as  $h \rightarrow 0^+$*

$$\begin{aligned} & \partial_x^{h,2} f_{i,j} = f_{xx}(x_i, y_j) + O(h^2), \quad \partial_y^{h,2} f_{i,j} = f_{yy}(x_i, y_j) + O(h^2), \\ & \quad \quad \quad \partial_{xy}^{h,2} f_{i,j} = f_{xy}(x_i, y_j) + O(h^2), \\ & \quad \quad \quad \nabla^h f_{i,j} = \nabla f(x_i, y_j) + O(h^2), \\ & \quad \quad \quad \partial_x f_{n+1,k}^h = f_x(a+c, y_k) + O(h^2), \\ & \quad \quad \quad |O(h^2)| \leq C \|f\|_{C^4(\bar{\Omega})} h^2, \\ & \quad \quad \quad i, j = 1, \dots, n; \quad k = 0, \dots, n+1. \end{aligned}$$

We have for any function  $f \in C^1(\bar{\Omega})$ :

$$(4.10) \quad \int_{\Omega} f(\mathbf{x}) dx = \int_{\Omega,rt} f(\mathbf{x}_{i,j}^h) d\mathbf{x}_{i,j}^h + O(h), \quad |O(h)| \leq C \|f\|_{C^1(\bar{\Omega})} h,$$

where the symbol

$$\int_{\Omega,rt} f(\mathbf{x}_{i,j}^h) d\mathbf{x}_{i,j}^h$$

denotes the approximation of the regular integral in (4.10) by the rectangle method, i.e.

$$(4.11) \quad \int_{\Omega,rt} f(\mathbf{x}_{i,j}^h) d\mathbf{x}_{i,j}^h = h^2 \sum_{i,j=0}^{n+1} f^2(x_i, y_j), \quad \forall f \in C^1(\bar{\Omega}).$$

Even though the rectangle method works for a more general set of functions  $f(\mathbf{x})$ , it is convenient for the goal of this paper to restrict our attention in (4.11) only to functions  $f \in C^1(\overline{\Omega})$ .

**4.2. Some function spaces.** First, we introduce some discrete analogs of two function spaces  $L_2(\Omega)$  and  $H^2(\Omega)$ . We set for all functions  $f(\mathbf{x})$  defined at all points of the domain  $\Omega$ :

$$(4.12) \quad L_2^h(\Omega^h) = \left\{ f^h : \|f^h\|_{L_2^h(\Omega^h)}^2 = \int_{\Omega, rt} f^2(\mathbf{x}_{ij}^h) d\mathbf{x}_{ij}^h = h^2 \sum_{i,j=0}^{n+1} f^2(x_i, y_j) \right\}.$$

$$(4.13) \quad H^{2,h}(\Omega^h) = \left\{ \begin{array}{l} f^h : \|f^h\|_{H^{2,h}(\Omega^h)}^2 = \|f^h\|_{L_2^h(\Omega^h)}^2 + \\ + h^2 \sum_{i,j=1}^n [(\partial_x^h f_{i,j})^2 + (\partial_y^h f_{i,j})^2] + \\ + h^2 \sum_{i,j=1}^n [(\partial_x^{h,2} f_{i,j})^2 + (\partial_y^{h,2} f_{i,j})^2 + (\partial_{yy}^h f_{i,j}^h)^2] \end{array} \right\}.$$

Clearly, sums in (4.13) are approximate values of integrals over  $\Omega$  of corresponding functions calculated by the rectangle rule (4.11). Hence, by Proposition 4.1 and (4.10)-(4.14)

$$(4.14) \quad \begin{aligned} \|f^h\|_{L_2^h(\Omega^h)}^2 &= \|f\|_{L_2(\Omega)}^2 + O(h) \text{ as } h \rightarrow 0^+, \forall f \in C^1(\overline{\Omega}), \\ |O(h)| &\leq C \|f\|_{C^1(\overline{\Omega})}^2 h. \end{aligned}$$

$$(4.15) \quad \begin{aligned} \|f^h\|_{H^{2,h}(\Omega^h)}^2 &= \|f\|_{H^2(\Omega)}^2 + O(h) \text{ as } h \rightarrow 0^+, \forall f \in C^4(\overline{\Omega}), \\ |O(h)| &\leq C \|f\|_{C^4(\overline{\Omega})}^2 h. \end{aligned}$$

Recalling that the spaces  $H_{1,\theta}$  and  $H_{1,2,\theta}$  are defined in (3.20), introduce six more function spaces:

$$(4.16) \quad H_{1,2,\theta,fd} = \left\{ \begin{array}{l} (q^h, p^h)(\mathbf{x}_{i,j}^h, \theta) : q^h, p^h \in H^{2,h}(\Omega^h), \\ \|(q^h, p^h)(\mathbf{x}_{i,j}^h, \theta)\|_{H_{1,2,\theta,fd}}^2 = \\ = \|q^h(\mathbf{x}_{i,j}^h, \theta)\|_{H^{2,h}(\Omega^h)}^2 + \|p^h(\mathbf{x}_{i,j}^h, \theta)\|_{H^{2,h}(\Omega^h)}^2 < \infty, \\ \forall \theta \in [0, 2\pi], \end{array} \right\},$$

$$(4.17) \quad H_{1,2,2,\theta,fd} = \left\{ \begin{array}{l} (q^h, p^h, q, p) : \\ (q^h, p^h) \in H_{1,2,\theta,fd}, (q, p) \in H_{1,2,\theta}, \\ (q^h, p^h)(x_i, y_j, \theta) = (q, p)(x_i, y_j, \theta), \\ i, j = 0, \dots, n+1, \\ \|(q^h, p^h, q, p)\|_{H_{1,2,2,\theta,fd}}^2 = \\ = \|(q^h, p^h)\|_{H_{1,2,\theta,fd}}^2 + \|(q, p)\|_{H_{1,2,\theta}}^2, \\ \forall \theta \in [0, 2\pi], \end{array} \right\}$$

$$(4.18) \quad H_{1,2,\theta,fd}^0 = (q^h, p^h) : \left\{ \begin{array}{l} q^h(\mathbf{x}_{i,j}^h, \theta)|_{\partial\Omega^h} = p^h(\mathbf{x}_{i,j}^h, \theta)|_{\partial\Omega^h} = 0, \\ i, j = 0, \dots, n+1, \\ \partial_x q_{n+1,k}^h = \partial_x p_{n+1,k}^h = 0, k = 0, \dots, n+1, \\ \text{see (4.7) for } \partial_x q_{n+1,k}^h, \partial_x p_{n+1,k}^h, \\ \|\cdot\|_{H_{1,2,\theta,fd}^0} = \|\cdot\|_{H_{1,2,\theta,fd}} \end{array} \right\},$$

$$(4.19) \quad H_{1,2,2,\theta,fd}^0 = \left\{ \begin{array}{l} (q^h, p^h, q, p) \in H_{1,2,2,\theta,fd} : \\ (q^h, p^h) \in H_{1,2,\theta,fd}^0, (q, p) \in H_{1,2,\theta}^0, \\ \|\cdot\|_{H_{1,2,2,\theta,fd}^0} = \|\cdot\|_{H_{1,2,2,\theta,fd}}, \quad \forall \theta \in [0, 2\pi] \end{array} \right\},$$

$$(4.20) \quad H_{1,2,\theta}^2 = \left\{ \begin{array}{l} (q, p) (\mathbf{x}, \theta) \in H^2(\Omega) \times H^2(\Omega) : \\ \|(q, p) (\mathbf{x}, \theta)\|_{H_{1,2,\theta}^2}^2 = \|q (\mathbf{x}, \theta)\|_{H^2(\Omega)}^2 + \|p (\mathbf{x}, \theta)\|_{H^2(\Omega)}^2, \\ \forall \theta \in [0, 2\pi]. \end{array} \right\}$$

$$(4.21) \quad H_{1,2,2,\theta,fd}^2 = \left\{ \begin{array}{l} (q^h, p^h, q, p) : \\ (q^h, p^h) \in H_{1,2,\theta,fd}, (q, p) \in H_{1,2,\theta}^2, \\ \|(q^h, p^h, q, p)\|_{H_{1,2,2,\theta,fd}^2} = \\ = \|(q^h, p^h)\|_{H_{1,2,\theta,fd}}^2 + \|(q, p)\|_{H_{1,2,\theta}^2}^2 \quad \forall \theta \in [0, 2\pi]. \end{array} \right\},$$

Recall that the space  $H_{1,2,\theta}$  was defined in (3.20). Keeping in mind (4.3), we define now the semi-discrete analog  $G_\theta^h(A)$  of the set  $G_\theta(A)$  in (3.22) as:

**Definition.**  $G_\theta^h(A)$  is the set of all vector functions  $(q^h, p^h, q, p) \in H_{1,2,2,\theta,fd}$  such that  $(q, p) \in G_\theta(A)$ . Boundary conditions (3.13), (3.15) for  $(q^h, p^h)$  at  $(x_{n+1}, y_j) = (a+c, y_j)$  are understood in terms of (4.7).

Hence, by (4.14), (4.15), (4.16), (4.20) and (4.21)

$$(4.22) \quad G_\theta^h(A) \subset H_{1,2,2,\theta,fd},$$

$$(4.23) \quad \begin{aligned} \|(q^h, p^h)\|_{H_{1,2,\theta,fd}}^2(\theta) &= \|(q, p)\|_{H_{1,2,\theta}^2}^2(\theta) + O(h), \\ \forall (q^h, p^h, q, p) &\in G_\theta^h(A), \quad \forall \theta \in [0, 2\pi]. \end{aligned}$$

Thus, using (3.12)-(3.15), (3.16), (3.22), (4.4), (4.3), (4.7), Definition, (4.16), (4.17) and (4.22), we obtain

$$(4.24) \quad \begin{aligned} q^h(x_i, y_j, \theta) |_{(x_i, y_j) \in \partial\Omega^h} &= \partial_\theta s_0(x_i, y_j, \theta), \\ \partial_x^h q^h(x_{n+1}, y_j, \theta) &= \partial_\theta s_1(x_{n+1}, y_j, \theta), \quad (x_{n+1}, y_j) \in \Gamma_0, \\ p^h(x_i, y_j, \theta) |_{(x_i, y_j) \in \partial\Omega^h} &= (\partial_\theta s_0 - \varepsilon s_0)(x_i, y_j, \theta), \\ \partial_x^h p^h(x_{n+1}, y_j, \theta) &= (\partial_\theta s_1 - \varepsilon s_1)(x_{n+1}, y_j, \theta), \quad (x_{n+1}, y_j) \in \Gamma_0, \\ & \quad i, j = 0, \dots, n+1, \\ \forall (q^h, p^h, q, p) &\in G_\theta^h(A), \quad \forall \theta \in [0, 2\pi], \end{aligned}$$

where  $\partial_x^h q^h(x_{n+1}, y_j, \theta)$  and  $\partial_x^h p^h(x_{n+1}, y_j, \theta)$  are understood in terms of (4.7).

**4.3. Semi-discretization of the functional  $J_{\kappa,\alpha}$ .** First, using (4.16), we consider the discrete analog  $J_{1,h,\kappa,\alpha}$  of the functional  $J_{1,\kappa,\alpha}$  in (3.41),

$$(4.25) \quad \begin{aligned} &J_{1,h,\kappa,\alpha}(q^h, p^h)(\theta) = \\ &= \sqrt{\varepsilon} \int_{\Omega, \tau t} \left[ (F_1^h(q^h, p^h)(\mathbf{x}_{i,j}^h, \theta))^2 + (F_2^h(q^h, p^h)(\mathbf{x}_{i,j}^h, \theta))^2 \right] W_\kappa^h(\mathbf{x}_{i,j}^h) d\mathbf{x}_{i,j}^h, \end{aligned}$$

$$\forall (q^h, p^h) (\mathbf{x}_{i,j}^h, \theta) \in H_{1,2,\theta,fd}, \forall \theta \in [0, 2\pi].$$

Operators  $F_1^h, F_2^h$  in (4.25) are finite difference versions of operators  $F_1, F_2$  in (3.10), (3.11). Next, the functional

$$(4.26) \quad J_{2,\kappa,\alpha}(q, p)(\theta) \text{ remains the same as in (3.42).}$$

Now, using (4.17), (4.22), (4.25) and (4.26) and Definition, we define the semi-discrete analog of the functional  $J_{\kappa,\alpha}(q, p)(\theta)$  similarly with (3.43) as:

$$(4.27) \quad \begin{aligned} J_{h,\kappa,\alpha}(q^h, p^h, q, p)(\theta) &= J_{1,h,\kappa,\alpha}(q^h, p^h)(\theta) + J_{2,\kappa,\alpha}(q, p)(\theta), \\ \forall (q^h, p^h, q, p) &\in G_\theta^h(A), \forall \theta \in [0, 2\pi]. \end{aligned}$$

## 5. Theorems About the Semi-Discrete Functional $J_{h,\kappa,\alpha}$ .

**5.1. The  $h$ -strong convexity of  $J_{h,\kappa,\alpha}$ .** Below  $\{, \}$  and  $[, ]$  are scalar products in  $H_{1,2,2,\theta,fd}$  and  $H_{1,2,\theta}$  respectively.

**Theorem 5.1** (the  $h$ -strong convexity). *The following hold true:*

1. For each  $\kappa > 0$ , for each  $\theta \in [0, 2\pi]$  and for each vector function  $(q^h, p^h, q, p) \in \overline{G_\theta^h(A)}$  the functional  $J_{h,\kappa,\alpha}(q^h, p^h, q, p)(\theta)$  has the Fréchet derivative

$$(5.1) \quad J'_{h,\kappa,\alpha}(q^h, p^h, q, p)(\theta) \in H_{1,2,2,\theta,fd}^0,$$

where  $H_{1,2,2,\theta,fd}^0$  is the function space defined in (4.18). Furthermore,

$$(5.2) \quad \begin{aligned} &J'_{h,\kappa,\alpha}(q_1^h, p_1^h, q_1, p_1)(\theta) (q_2^h - q_1^h, p_2^h - p_1^h, q_2 - q_1, p_2 - p_1) (x_{i,j}^h, \theta) = \\ &= J'_{\kappa,\alpha}(q_1, p_1)(\theta) (q_2 - q_1, p_2 - p_1) + O(h) \exp\left(2\kappa(a+c)^2\right), \end{aligned}$$

$$\forall (q_1^h, p_1^h, q_1, p_1), (q_2^h, p_2^h, q_2, p_2) \in G_\theta^h(A), \forall \theta \in [0, 2\pi],$$

where  $J'_{\kappa,\alpha}(q, p)(\theta)$  is the Fréchet derivative of the functional  $J_{\kappa,\alpha}(q, p)(\theta)$ , which was found in Theorem 3.2.

2. Let  $\kappa_0 = \kappa_0(\Omega) \geq 1$  and  $\kappa_1 = \kappa_1(A, \Omega, \varepsilon) \geq \kappa_0$  be the numbers of Theorems 3.1 and 3.2 respectively. Then there exists a sufficiently large number  $\kappa_2 = \kappa_2(A, \Omega, \varepsilon) \geq \kappa_1$  such that for each  $\kappa \geq \kappa_2$  and for each  $\theta \in [0, 2\pi]$  the functional  $J_{h,\kappa,\alpha}(q^h, p^h, q, p)(\theta)$  is  $h$ -strongly convex on the set  $\overline{G_\theta^h(A)}$ , i.e.

$$(5.3) \quad \begin{aligned} &J_{h,\kappa,\alpha}(q_2^h, p_2^h, q_2, p_2)(\theta) - J_{h,\kappa,\alpha}(q_1^h, p_1^h, q_1, p_1)(\theta) - \\ &- J'_{h,\kappa,\alpha}(q_1^h, p_1^h, q_1, p_1)(\theta) (q_2^h - q_1^h, p_2^h - p_1^h, q_2 - q_1, p_2 - p_1) \geq \\ &\geq C_1 \exp\left(2\kappa(a-c)^2\right) \|(q_2^h - q_1^h, p_2^h - p_1^h)\|_{H_{1,2,\theta,fd}}^2 + \\ &+ \alpha \|(q_2 - q_1, p_2 - p_1)\|_{H_{1,2,\theta}}^2 - C_1 h \exp\left(2\kappa(a+c)^2\right), \\ &\forall (q_1^h, p_1^h, q_1, p_1), (q_2^h, p_2^h, q_2, p_2) \in \overline{G_\theta^h(A)}, \\ &\forall \theta \in [0, 2\pi], \forall \kappa \geq \kappa_2. \end{aligned}$$

3. Assume that there exists a pair of numbers  $(\kappa_3, \theta_0)$  satisfying  $\kappa_3 \geq \kappa_2$ ,  $\theta_0 \in [0, 2\pi]$  and such that there exists a minimizer

$$(5.4) \quad X_{\min} = (\tilde{q}_{\min, \kappa_3, \alpha}^h, \tilde{p}_{\min, \kappa_3, \alpha}^h, \tilde{q}_{\min, \kappa_3, \alpha}^h, \tilde{p}_{\min, \kappa_3, \alpha}^h) \in \overline{G_{\theta_0}^h(A)}$$

of the functional  $J_{h, \kappa_3, \alpha}(q^h, p^h, q, p)(\theta_0)$  on the set  $\overline{G_{\theta_0}^h(A)}$ . In other words, assume that

$$(5.5) \quad \begin{aligned} J_{h, \kappa_3, \alpha}(X_{\min})(\theta_0) &\leq J_{h, \kappa, \alpha}(q^h, p^h, q, p)(\theta_0), \\ \forall (q^h, p^h, q, p)(\theta_0) &\in G_{\theta_0}^h(A). \end{aligned}$$

Then

$$(5.6) \quad \begin{aligned} J'_{h, \kappa_3, \alpha}(X_{\min})(X_{\min} - (q^h, p^h, q, p))(\theta_0) &\leq 0, \\ \forall (q^h, p^h, q, p) &\in G_{\theta_0}^h(A). \end{aligned}$$

**Proof.** For every  $\theta \in [0, 2\pi]$  define the set  $G_{\theta, 0}^h(2A)$  similarly with the set  $G_{\theta}^h(A)$  in Definition. More precisely,

$$(5.7) \quad \begin{aligned} G_{\theta, 0}^h(2A) &\text{ is defined the same way as } G_{\theta}^h(A) \text{ in Definition,} \\ &\text{except that } A \text{ is replaced with } 2A, \\ &\text{and the right hand sides of boundary conditions} \\ &\text{(3.12)-(3.15) are replaced with zeros.} \end{aligned}$$

Then (4.16)-(4.22) and (5.7) imply

$$(5.8) \quad \overline{G_{\theta, 0}^h(2A)} \subset H_{1, 2, 2, \theta, fd}^0.$$

Let  $(q_1^h, p_1^h, q_1, p_1) \in \overline{G_{\theta}^h(A)}$  and  $(q_2^h, p_2^h, q_2, p_2) \in \overline{G_{\theta}^h(A)}$  be two arbitrary pairs. Denote

$$(5.9) \quad (m^h, z^h, m, z) = (q_2^h, p_2^h, q_2, p_2) - (q_1^h, p_1^h, q_1, p_1).$$

Then, using (5.7), we obtain

$$(5.10) \quad (m^h, z^h, m, z) \in \overline{G_{\theta, 0}^h(2A)}.$$

By (3.10), (3.16) and (4.9)

$$(5.11) \quad F_1^h(q^h, p^h)(x_i, y_j, \theta) = \Delta^h q_{i,j}(\theta) + 2\nabla^h q_{i,j}(\theta) \nabla^h \left( \frac{q_{i,j} - p_{i,j}}{\varepsilon} \right)(\theta).$$

Hence, using (5.7), we obtain

$$\begin{aligned} F_1^h((q_2^h, p_2^h)(x_i, y_j, \theta)) &= F_1^h((q_1^h + m^h, p_1^h + z^h)(x_i, y_j, \theta)) = \\ &= F_1^h((q_1^h, p_1^h)(x_i, y_j, \theta)) + \\ &+ (\Delta^h m_{i,j}(\theta) + 2\nabla^h q_{1,i,j}(\theta) \nabla^h((m_{i,j} - z_{i,j})/\varepsilon)) + \\ &+ 2\nabla^h m_{i,j}(\theta) \nabla^h((q_{1,i,j} - p_{1,i,j})/\varepsilon)(\theta) + \\ &+ 2\nabla^h m_{i,j}(\theta) \nabla^h((m_{i,j} - z_{i,j})/\varepsilon)(\theta). \end{aligned}$$

Hence,

$$(5.12) \quad \begin{aligned} [F_1^h((q_2^h, p_2^h)(x_i, y_j, \theta))]^2 &- [F_1^h((q_1^h, p_1^h)(x_i, y_j, \theta))]^2 = \\ &= L_{1, \text{lin}, h}((m^h, z^h)(x_i, y_j, \theta)) + \\ &+ L_{1, \text{nonlin}, h}((m^h, z^h)(x_i, y_j, \theta)). \end{aligned}$$

In (5.12) terms  $L_{1,\text{lin},h}((m^h, z^h)(x_i, y_j, \theta))$  and

$L_{1,\text{nonlin},h}((m^h, z^h)(x_i, y_j, \theta))$  are linear and nonlinear ones respectively with respect to  $(m^h, z^h)(x_i, y_j, \theta)$ . More precisely,

$$(5.13) \quad L_{1,\text{lin},h}((m^h, z^h)(x_i, y_j, \theta)) = 2F_1^h((q_1^h, p_1^h)(x_i, y_j, \theta)) \times \\ \times \left[ \begin{array}{l} \Delta^h m_{i,j}(\theta) + 2\nabla^h q_{1,i,j}(\theta) \nabla^h((m_{i,j} - z_{i,j})/\varepsilon)(\theta) + \\ + 2\nabla^h m_{i,j}(\theta) \nabla^h((q_{1,i,j} - p_{1,i,j})/\varepsilon)(\theta) \end{array} \right].$$

$$(5.14) \quad L_{1,\text{nonlin},h}((m^h, z^h)(x_i, y_j, \theta)) = \\ = \left[ \begin{array}{l} (\Delta^h m_{i,j}(\theta) + 2\nabla^h q_{1,i,j}(\theta) \nabla^h((m_{i,j} - z_{i,j})/\varepsilon)(\theta) + \\ + 2\nabla^h m_{i,j}(\theta) \nabla^h((q_{1,i,j} - p_{1,i,j})/\varepsilon)(\theta) + \\ + 2\nabla^h m_{i,j}(\theta) \nabla^h((m_{i,j} - z_{i,j})/\varepsilon)(\theta) \end{array} \right]^2 + \\ + 4F_1^h((q_1^h, p_1^h)(x_i, y_j, \theta)) \cdot \nabla^h m_{i,j}(\theta) \nabla^h((m_{i,j} - z_{i,j})/\varepsilon)(\theta).$$

Using (4.11), (5.7)-(5.10) and (5.14), we obtain

$$(5.15) \quad \sqrt{\varepsilon} \int_{\Omega,rt} \left| L_{1,\text{nonlin},h}((m^h, z^h)(\mathbf{x}_{i,j}^h, \theta)) \right| W_\kappa^h(\mathbf{x}_{i,j}^h) d\mathbf{x}_{i,j}^h \leq \\ \leq C_1 \exp\left(2\kappa(a+c)^2\right) \|(m^h, z^h)(\mathbf{x}_{i,j}^h, \theta)\|_{H_{1,2,\theta,fd}}^2.$$

Obviously an expression, which is similar with the one in (5.12), is valid for the term  $[F_2^h((q_2^h, p_2^h)(x_i, y_j, \theta))]^2 - [F_2^h(q_1^h, p_1^h)(x_i, y_j, \theta)]^2$ . In this case

$L_{1,\text{lin},h}((m^h, z^h)(x_i, y_j, \theta))$  and  $L_{1,\text{nonlin},h}((m^h, z^h)(x_i, y_j, \theta))$  are replaced with slightly different operators  $L_{2,\text{lin},h}((m^h, z^h)(x_i, y_j, \theta))$  and  $L_{2,\text{nonlin},h}((m^h, z^h)(x_i, y_j, \theta))$  respectively, and analogs of formulas (5.13)-(5.15) are valid.

Thus, (4.25), (4.26), (5.10) and (5.13)-(5.15) imply

$$(5.16) \quad J_{h,\kappa,\alpha}(q_2^h, p_2^h, q_2, p_2)(\theta) - J_{h,\kappa,\alpha}(q_1^h, p_1^h, q_1, p_1)(\theta) = \\ = \sqrt{\varepsilon} \int_{\Omega_{rt}} L_{1,\text{lin},h}((m^h, z^h)(\mathbf{x}_{i,j}^h, \theta)) W_\kappa^h(\mathbf{x}_{i,j}^h) d\mathbf{x}_{i,j}^h + \\ + \sqrt{\varepsilon} \int_{\Omega_{rt}} L_{2,\text{lin},h}((m^h, z^h)(\mathbf{x}_{i,j}^h, \theta)) W_\kappa^h(\mathbf{x}_{i,j}^h) d\mathbf{x}_{i,j}^h + \\ + 2[(q_1, p_1), (m, z)](\mathbf{x}, \theta) + \\ + \sqrt{\varepsilon} \int_{\Omega_{rt}} L_{1,\text{nonlin},h}((m^h, z^h)(\mathbf{x}_{i,j}^h, \theta)) W_\kappa^h(\mathbf{x}_{i,j}^h) d\mathbf{x}_{i,j}^h + \\ + \sqrt{\varepsilon} \int_{\Omega_{rt}} L_{2,\text{nonlin},h}((m^h, z^h)(\mathbf{x}_{i,j}^h, \theta)) W_\kappa^h(\mathbf{x}_{i,j}^h) d\mathbf{x}_{i,j}^h + \\ + \|(m, z)(\mathbf{x}, \theta)\|_{H_{1,2,\theta}}^2, \quad \forall \theta \in [0, 2\pi], \forall \kappa \geq \kappa_2.$$

Keeping in mind (4.16)-(4.19) and (5.7)-(5.10), consider the functional

$$\begin{aligned}
& P^h(\theta) : H_{1,2,2,\theta,fd}^0 \rightarrow \mathbb{R}, \\
& P(t_1^h, t_2^h, t_1, t_2)(\theta) = \sqrt{\varepsilon} \int_{\Omega_{rt}} L_{1,\text{lin},h}((t_1^h, t_2^h)(\mathbf{x}_{i,j}^h, \theta)) W_\kappa^h(\mathbf{x}_{i,j}^h) d\mathbf{x}_{i,j}^h + \\
(5.17) \quad & + \sqrt{\varepsilon} \int_{\Omega_{rt}} L_{2,\text{lin},h}((t_1^h, t_2^h)(\mathbf{x}_{i,j}^h, \theta)) W_\kappa^h(\mathbf{x}_{i,j}^h) d\mathbf{x}_{i,j}^h + \\
& + 2[(q_1, p_1), (t_1, t_2)], \\
& \forall (t_1^h, t_2^h, t_1, t_2) \in H_{1,2,2,\theta,fd}^0, \forall \theta \in [0, 2\pi].
\end{aligned}$$

This is a bounded linear functional defined on the Hilbert space  $H_{1,2,2,\theta,fd}^0$ . Hence, by Riesz theorem for each  $\theta \in [0, 2\pi]$  there exists unique point  $\widehat{P}^h(\theta) \in H_{1,2,2,\theta,fd}^0$  such that

$$\begin{aligned}
(5.18) \quad & P^h(t_1^h, t_2^h, t_1, t_2)(\theta) = \left\{ \widehat{P}^h(\theta), (t_1^h, t_2^h, t_1, t_2) \right\}, \\
& \forall (t_1^h, t_2^h, t_1, t_2) \in H_{1,2,2,\theta,fd}^0, \forall \theta \in [0, 2\pi].
\end{aligned}$$

It follows from (3.20), (4.16)-(4.19), (5.9) and (5.15)-(5.18) that

$$\begin{aligned}
& \left| J_{h,\kappa,\alpha}(q_2^h, p_2^h, q_2, p_2)(\theta) - J_{h,\kappa,\alpha}(q_1^h, p_1^h, q_1, p_1)(\theta) - \right. \\
& \left. - \left\{ \widehat{P}^h(\theta), (q_2^h - q_1^h, p_2^h - p_1^h, q_2 - q_1, p_2 - p_1)(\mathbf{x}_{i,j}^h, \theta) \right\} \right| \leq \\
& \leq C_1 \left\| (q_2^h - q_1^h, p_2^h - p_1^h, q_2 - q_1, p_2 - p_1) \right\|_{H_{1,2,2,\theta,fd}^0}^2, \forall \theta \in [0, 2\pi].
\end{aligned}$$

Hence,  $\widehat{P}^h(\theta) = J'_{h,\kappa,\alpha}(q_1^h, p_1^h, q_1, p_1)(\theta) \in H_{1,2,2,\theta,fd}^0$  is the Fréchet derivative of the functional  $J_{h,\kappa,\alpha}(q_1^h, p_1^h, q_1, p_1)(\theta)$  at an arbitrary point  $(q_1^h, p_1^h, q_1, p_1)(\theta) \in \overline{G_\theta^h(A)}$ , which proves (5.1).

We now prove (5.2). Using (3.18) and (4.11), we obtain

$$\begin{aligned}
& \sqrt{\varepsilon} \int_{\Omega_{rt}} L_{1,\text{lin},h}((m^h, z^h)(\mathbf{x}_{i,j}^h, \theta)) W_\kappa^h(\mathbf{x}_{i,j}^h) d\mathbf{x}_{i,j}^h = \\
(5.19) \quad & = \sqrt{\varepsilon} h^2 \sum_{i,j=1}^n 2F_1((q_1, p_1)(x_{1,i}, x_{2,j}, \theta)) \times \\
& \times \left[ \frac{\Delta^h m + 2\nabla^h q_1 \nabla^h((m - z)/\varepsilon) +}{+ 2\nabla^h m \nabla^h((q_1 - p_1)/\varepsilon)(\theta)} \right] (x_i, y_j, \theta) W_\kappa(x_i).
\end{aligned}$$

Hence, (4.2), (4.10), Proposition 4.1 and (5.19) imply

$$\sqrt{\varepsilon} \int_{\Omega_{rt}} L_{1,\text{lin},h}((m^h, z^h)(\mathbf{x}_{i,j}^h, \theta)) W_\kappa^h(\mathbf{x}_{i,j}^h) d\mathbf{x}_{i,j}^h =$$

$$(5.20) \quad = \sqrt{\varepsilon} \int_{\Omega} 2F_1((q_1, p_1)(\mathbf{x}, \theta)) \times \\ \times [\Delta m + 2\nabla q_1 \nabla((m-z)/\varepsilon) + 2\nabla m \nabla((q_1 - p_1)/\varepsilon)](\mathbf{x}, \theta) W_{\kappa}(\mathbf{x}) d\mathbf{x} + \\ + O(h) \exp(2\kappa(a+c)^2), \quad \forall \theta \in [0, 2\pi].$$

A similar formula and in a similar way can also be obtained for

$$(5.21) \quad \sqrt{\varepsilon} \int_{\Omega_{rt}} L_{2,\text{lin},h}((m^h, z^h)(\mathbf{x}_{i,j}^h, \theta)) W_{\kappa}^h(\mathbf{x}_{i,j}^h) d\mathbf{x}_{i,j}^h.$$

Comparison of (5.20) and its analog for (5.21) with the analogous formula (6.3) for the continuous case in [25] shows that (5.2) holds true.

Acting similarly, we obtain

$$(5.22) \quad J_{h,\kappa,\alpha}(q^h, p^h, q, p)(\theta) = J_{\kappa,\alpha}(q, p)(\theta) + O(h) \exp(2\kappa(a+c)^2), \\ \forall (q^h, p^h, q, p) \in G_{\theta}^h(A), \quad \forall \theta \in [0, 2\pi].$$

Comparing (5.2) and (5.22) with the continuous case of (3.26), we obtain the desired  $h$ -strong convexity property (5.3).

We now prove (5.6). Suppose that the opposite is true. In other words, assume that there exists a point  $(q^h, p^h, q, p) \in G_{\theta_0}^h(A)$  such that

$$(5.23) \quad J'_{h,\kappa_3,\alpha}(X_{\min})(X_{\min} - (q^h, p^h, q, p))(\theta_0) > 0.$$

Denote

$$(5.24) \quad Y = (q^h, p^h, q, p) \in G_{\theta_0}^h(A).$$

Then (5.4), (5.23) and (5.24) imply

$$(5.25) \quad J'_{h,\kappa,\alpha}(X_{\min})(X_{\min} - Y) > 0.$$

Consider the interval of the straight line connecting points  $\tilde{Z}_{\min}$  and  $Y$ . This interval is

$$I = \{(1-\beta)X_{\min} + \beta Y, \beta \in [0, 1]\}.$$

Since the set  $\overline{G_{\theta_0}^h(A)}$  is convex, then  $I \in \overline{G_{\theta_0}^h(A)}$ . This is equivalent with

$$X_{\min} + \beta(Y - X_{\min}) \in \overline{G_{\theta_0}^h(A)}, \quad \forall \beta \in [0, 1].$$

We have for sufficiently small  $\beta > 0$ :

$$(5.26) \quad J_{h,\kappa_3,\alpha}(X_{\min} + \beta(Y - X_{\min}))(\theta_0) = J_{h,\kappa_3,\alpha}(X_{\min})(\theta_0) + \\ + J'_{h,\kappa_3,\alpha}(X_{\min})(\beta(Y - X_{\min}))(\theta_0) + o(1), \quad \text{as } \beta \rightarrow 0^+.$$

Using (5.25), we obtain

$$J'_{h,\kappa_3,\alpha}(X_{\min})(\beta(Y - X_{\min}))(\theta_0) = \beta J'_{h,\kappa_3,\alpha}(X_{\min})(Y - X_{\min})(\theta_0) < 0.$$

Hence, (5.26) implies that for sufficiently small values of  $\beta > 0$

$$(5.27) \quad J_{h,\kappa_3,\alpha}(X_{\min} + \beta(Y - X_{\min}))(\theta_0) < J_{h,\kappa_3,\alpha}(X_{\min})(\theta_0).$$

However, (5.27) contradicts to (5.5).  $\square$

**5.2. Accuracy estimates.** The following accuracy estimates take place.

**Theorem 5.2.** *Assume that conditions of Theorems 3.3 and 5.1 hold. In particular, let  $\kappa_3$  and  $\theta_0$  be the pair of numbers of item 3 of Theorem 5.1 and let*

*$(q_{\min, \kappa_3, \alpha}, p_{\min, \kappa_3, \alpha})(\mathbf{x}, \theta_0) \in \overline{G_{\theta_0}(A)}$  be the corresponding minimizer of the functional  $J_{\kappa_3, \alpha}(q, p)(\theta)$  on the set  $\overline{G_{\theta_0}(A)}$ . Let*

$$(5.28) \quad Z_{\min} = (q_{\min, \kappa_3, \alpha}^h, p_{\min, \kappa_3, \alpha}^h, q_{\min, \kappa_3, \alpha}, p_{\min, \kappa_3, \alpha}) \in \overline{G_{\theta_0}^h(A)}$$

*be the corresponding point of the space  $H_{1,2,2,\theta_0,fd}$ . Also, let  $X_{\min} \in \overline{G_{\theta_0}^h(A)}$  be the minimizer (5.4) of the functional  $J_{h, \kappa_3, \alpha}(q^h, p^h, q, p)(\theta_0)$  on the set  $\overline{G_{\theta_0}^h(A)}$ , which was mentioned in item 3 of Theorem 5.1. Denote*

$$(5.29) \quad Z^* = (q^{*h}, p^{*h}, q^*, p^*) \in G_{\theta_0}^h(A),$$

*see item 2 of Theorem 3.3 and, in particular, (3.38) about the pair  $(q^*, p^*)(\mathbf{x}, \theta_0) \in G_{\theta_0}(A)$ . Then the following accuracy estimates hold*

$$(5.30) \quad \|Z_{\min} - X_{\min}\|_{H_{1,2,2,\theta_0,fd}^2} \leq C_1 (\sqrt{\alpha} + \sqrt{h}) \exp(\kappa_3(a+c)^2),$$

$$(5.31) \quad \|Z^* - X_{\min}\|_{H_{1,2,2,\theta_0,fd}^2} \leq C_1 (\sqrt{\alpha} + \sqrt{h}) \exp(\kappa_3(a+c)^2).$$

**Proof.** Using (4.21), (4.22), (5.4), (5.3) and (5.28), we obtain

$$(5.32) \quad \begin{aligned} & J_{h, \kappa_3, \alpha}(Z_{\min})(\theta_0) - J_{h, \kappa_3, \alpha}(X_{\min})(\theta_0) - \\ & - J'_{h, \kappa_3, \alpha}(X_{\min})(Z_{\min} - X_{\min})(\theta_0) \geq \\ & \geq C_1 \exp(2\kappa_3(a-c)^2) \|Z_{\min} - X_{\min}\|_{H_{1,2,2,\theta_0,fd}^2}^2 - \\ & - C_1 h \exp(2\kappa_3(a+c)^2). \end{aligned}$$

Since by (5.6)

$$-J_{h, \kappa, \alpha}(X_{\min})(\theta_0) - J'_{h, \kappa, \alpha}(X_{\min})(\theta_0)(Z_{\min} - X_{\min}) \leq 0,$$

then (5.32) implies

$$(5.33) \quad \begin{aligned} & J_{h, \kappa, \alpha}(Z_{\min})(\theta_0) \geq \\ & \geq C_1 \exp(2\kappa_3(a-c)^2) \|Z_{\min} - X_{\min}\|_{H_{1,2,2,\theta_0,fd}^2}^2 - \\ & - C_1 h \exp(2\kappa_3(a+c)^2). \end{aligned}$$

By (5.22) and (5.28)

$$J_{h, \kappa_3, \alpha}(Z_{\min})(\theta_0) = J_{\kappa_3, \alpha}(q_{\min, \kappa_3, \alpha}, p_{\min, \kappa_3, \alpha})(\theta_0) + O(h) \exp(2\kappa_3(a+c)^2).$$

Substituting this in (5.33), we obtain

$$(5.34) \quad \begin{aligned} & J_{\kappa_3, \alpha}(q_{\min, \kappa_3, \alpha}, p_{\min, \kappa_3, \alpha})(\theta_0) \geq \\ & \geq C_1 \exp(2\kappa_3(a-c)^2) \|Z_{\min} - X_{\min}\|_{H_{1,2,2,\theta_0,fd}^2}^2 - \\ & - C_1 h \exp(2\kappa_3(a+c)^2). \end{aligned}$$

It follows from (3.10), (3.11), (3.16) and (3.24) that

$$(5.35) \quad J_{\kappa,\alpha}(q + \widehat{q}, p + \widehat{p})(\theta) \leq C_1 J_{\kappa,\alpha}(q, p)(\theta) + C_1 J_{\kappa,\alpha}(\widehat{q}, \widehat{p})(\theta), \\ \forall (q, p), (\widehat{q}, \widehat{p}) \in \overline{G_\theta(A)}, \forall \kappa > 0, \forall \theta \in [0, 2\pi].$$

Hence, in (5.34)

$$(5.36) \quad J_{\kappa_3,\alpha}(q_{\min,\kappa_3,\alpha}, p_{\min,\kappa_3,\alpha})(\theta_0) = \\ = J_{\kappa_3,\alpha}((q_{\min,\kappa_3,\alpha}, p_{\min,\kappa_3,\alpha}) - (q^*, p^*) + (q^*, p^*))(\theta_0) \leq \\ \leq C_1 J_{\kappa_3,\alpha}((q_{\min,\kappa_3,\alpha} - q^*, p_{\min,\kappa_3,\alpha} - p^*))(\theta_0) + \\ + C_1 J_{\kappa_3,\alpha}(q^*, p^*)(\theta_0).$$

Hence, (3.44) and (5.36) imply

$$(5.37) \quad J_{\kappa_3,\alpha}(q_{\min,\kappa_3,\alpha}, p_{\min,\kappa_3,\alpha})(\theta_0) \leq \\ \leq C_1 J_{\kappa_3,\alpha}((q_{\min,\kappa_3,\alpha} - q^*, p_{\min,\kappa_3,\alpha} - p^*))(\theta_0) + C_1 \alpha.$$

Next, using again (3.10), (3.11), (3.16) and (3.24), we obtain

$$(5.38) \quad J_{\kappa_3,\alpha}((q_{\min,\kappa_3,\alpha} - q^*, p_{\min,\kappa_3,\alpha} - p^*))(\theta_0) \leq \\ \leq C_1 \exp\left(2\kappa_3(a+c)^2\right) \|(q_{\min,\kappa_3,\alpha} - q^*, p_{\min,\kappa_3,\alpha} - p^*)\|_{H_{1,2,\theta_0}^2}^2 + C_1 \alpha.$$

Hence, by (3.39) and (5.36)-(5.38)

$$(5.39) \quad J_{\kappa_3,\alpha}(q_{\min,\kappa_3,\alpha}, p_{\min,\kappa_3,\alpha})(\theta_0) \leq C_1 \alpha \exp\left(2\kappa_3(a+c)^2\right).$$

Comparing (5.39) with (5.34), we obtain the first target estimate (5.30) of this theorem.

We now prove (5.31). By triangle inequality and (5.30)

$$\|Z^* - X_{\min}\|_{H_{1,2,2,\theta_0,fd}^2} \leq \|Z^* - Z_{\min}\|_{H_{1,2,2,\theta_0,fd}^2} + \|Z_{\min} - X_{\min}\|_{H_{1,2,2,\theta_0,fd}^2} \leq \\ (5.40) \quad \leq \|Z^* - Z_{\min}\|_{H_{1,2,2,\theta_0,fd}^2} + C_1 \left(\sqrt{\alpha} + \sqrt{h}\right) \exp\left(\kappa_3(a+c)^2\right).$$

Next, by (5.7), (5.8), (5.28) and (5.29)

$$(q^{*h} - q_{\min,\kappa_3,\alpha}^h, p^{*h} - p_{\min,\kappa_3,\alpha}^h, q^* - q_{\min,\kappa_3,\alpha}, p^* - p_{\min,\kappa_3,\alpha}) \in \overline{G_{\theta_0}^h(2A)}.$$

Hence, using (4.22), (4.23) and (5.28), we obtain

$$(5.41) \quad \|Z^* - Z_{\min}\|_{H_{1,2,2,\theta_0,fd}^2} \leq \|(q^* - q_{\min,\kappa_3,\alpha}, p^* - p_{\min,\kappa_3,\alpha})\|_{H_{1,2,\theta_0}^2} + C_1 \sqrt{h}.$$

Combining (5.41) with (3.39), we obtain

$$(5.42) \quad \|Z^* - Z_{\min}\|_{H_{1,2,2,\theta_0,fd}^2} \leq C_1 \sqrt{\alpha} \exp\left[-\kappa(a-c)^2\right] + C_1 \sqrt{h}.$$

Combining (5.40) with (5.42), we obtain (5.31), which is the second target estimate of this theorem.  $\square$

**5.3. Minimizing sequence.** It is assumed in Theorem 5.2 that there exists such a pair of numbers  $\kappa_3$  and  $\theta_0$  for which there exists a minimizer  $Z_{\min}$  in (5.28) of the functional  $J_{h,\kappa,\alpha}(q^h, p^h, q, p)(\theta_0)$  on the set  $\overline{G_{\theta_0}^h(A)}$ . We present in this section an analog of Theorem 5.2 for the case when the assumption about the existence of a minimizer is not imposed.

Let  $\kappa_2 = \kappa_2(A, \Omega, \varepsilon) \geq 1$  be the number of Theorem 5.1. In particular, unlike Theorem 5.2, where the numbers  $\kappa_3 \geq \kappa_2$  and  $\theta_0 \in [0, 2\pi]$  are fixed, we assume here that  $\kappa \geq \kappa_2$  and  $\theta \in [0, 2\pi]$  are two arbitrary numbers. Denote

$$(5.43) \quad m(h, \kappa, \alpha, \varepsilon, A, \theta) = \inf_{\overline{G_{\theta}^h(A)}} J_{h,\kappa,\alpha}(q^h, p^h, q, p), \quad \forall \kappa \geq \kappa_2, \quad \forall \theta \in [0, 2\pi].$$

It follows from (5.43) that there exists a minimizing sequence  $\{(q_n^h, p_n^h, q_n, p_n)\}_{n=1}^{\infty} \subset \overline{G_{\theta}^h(A)}$  such that

$$(5.44) \quad \begin{aligned} \lim_{n \rightarrow \infty} J_{h,\kappa,\alpha}(q_n^h, p_n^h, q_n, p_n) &= m(h, \kappa, \alpha, \varepsilon, A, \theta), \\ J_{h,\kappa,\alpha}(q_n^h, p_n^h, q_n, p_n) &\geq m(h, \kappa, \alpha, \varepsilon, A, \theta), \quad \forall n \geq 1. \end{aligned}$$

Denote

$$(5.45) \quad Z_n = (q_n^h, p_n^h, q_n, p_n) \in \overline{G_{\theta}^h(A)}.$$

**Theorem 5.3.** *Assume that (5.29) is replaced with*

$$(5.46) \quad Z^* = (q^{*h}, p^{*h}, q^*, p^*) \in G_{\theta}^h(A), \quad \forall \theta \in [0, 2\pi].$$

Let  $\kappa \geq \kappa_2$  be an arbitrary number. Let  $(q_{\min,\kappa,\alpha}, p_{\min,\kappa,\alpha})(\mathbf{x}, \theta) \in \overline{G_{\theta}(A)}$  be the minimizer of the functional  $J_{\kappa,\alpha}(q, p)(\theta)$  on the set  $\overline{G_{\theta}(A)}$ , which was found in Theorem 3.2. Let  $\{(q_n^h, p_n^h, q_n, p_n)\}_{n=1}^{\infty} \subset \overline{G_{\theta}^h(A)}$  be the above minimizing sequence of the functional  $J_{h,\kappa,\alpha}(q^h, p^h, q, p)$  satisfying (5.44). Then for each  $\theta \in [0, 2\pi]$  there exists such an integer  $N = N(h, \kappa, \alpha, \varepsilon, A, \theta) > 1$  depending only on listed parameters that the following analogs of accuracy estimates (5.30) and (5.31) hold

$$(5.47) \quad \begin{aligned} &\|q_{\min,\kappa,\alpha} - q_n, p_{\min,\kappa,\alpha} - p_n\|_{H_{1,2,\theta}^2} \leq \\ &\leq C_1 \left( \sqrt{\alpha} + \sqrt{h} \right) \exp \left( \kappa (a + c)^2 \right), \quad \forall n \geq N, \end{aligned}$$

$$(5.48) \quad \begin{aligned} &\|q^* - q_n, p^* - p_n\|_{H_{1,2,\theta}^2} \leq \\ &\leq C_1 \left( \sqrt{\alpha} + \sqrt{h} \right) \exp \left( \kappa (a + c)^2 \right), \quad \forall n \geq N, \end{aligned}$$

$$(5.49) \quad \|Z^* - Z_n\|_{H_{1,2,2,\theta,fd}^2} \leq C_1 \left( \sqrt{\alpha} + \sqrt{h} \right) \exp \left( \kappa (a + c)^2 \right), \quad \forall n \geq N.$$

**Proof.** Using (5.3), we obtain

$$\begin{aligned} &J_{h,\kappa,\alpha}(q_n^h, p_n^h, q_n, p_n)(\theta) - J_{h,\kappa,\alpha}(q_{\min,\kappa,\alpha}^h, p_{\min,\kappa,\alpha}^h, q_{\min,\kappa,\alpha}, p_{\min,\kappa,\alpha})(\theta) - \\ &\quad - J'_{h,\kappa,\alpha}(q_{\min,\kappa,\alpha}^h, p_{\min,\kappa,\alpha}^h, q_{\min,\kappa,\alpha}, p_{\min,\kappa,\alpha})(\theta) \\ &\quad (q_n^h - q_{\min,\kappa,\alpha}^h, p_n^h - p_{\min,\kappa,\alpha}^h, q_n - q_{\min,\kappa,\alpha}, p_n - p_{\min,\kappa,\alpha}) \geq \end{aligned}$$

$$(5.50) \quad \geq C_1 \exp\left(2\kappa(a-c)^2\right) \|(q_n^h - q_{\min,\kappa,\alpha}^h, p_n^h - p_{\min,\kappa,\alpha}^h)\|_{H_{1,2,\theta,fd}}^2 + \\ + \alpha \|(q_n - q_{\min,\kappa,\alpha}, p_n - p_{\min,\kappa,\alpha})\|_{H_{1,2,\theta}}^2 - C_1 h \exp\left(2\kappa(a+c)^2\right), \quad \forall n \geq 1.$$

Next, by (4.23)

$$(5.51) \quad \|(q_n^h - q_{\min,\kappa,\alpha}^h, p_n^h - p_{\min,\kappa,\alpha}^h)\|_{H_{1,2,\theta,fd}}^2 \geq \\ \geq \|(q_n - q_{\min,\kappa,\alpha}, p_n - p_{\min,\kappa,\alpha})\|_{H_{1,2,\theta}^2}^2 - C_1 h, \quad \forall n \geq 1.$$

Also, by (5.2)

$$(5.52) \quad \begin{aligned} & -J'_{h,\kappa,\alpha}(q_{\min,\kappa,\alpha}^h, p_{\min,\kappa,\alpha}^h, q_{\min,\kappa,\alpha}, p_{\min,\kappa,\alpha})(\theta) \\ & (q_n^h - q_{\min,\kappa,\alpha}^h, p_n^h - p_{\min,\kappa,\alpha}^h, q_n - q_{\min,\kappa,\alpha}, p_n - p_{\min,\kappa,\alpha}) \geq \\ & \geq -J'_{\kappa,\alpha}(q_{\min,\kappa,\alpha}, p_{\min,\kappa,\alpha})(\theta) (q_n - q_{\min,\kappa,\alpha}, p_n - p_{\min,\kappa,\alpha}) - \\ & -C_1 h \exp\left(2\kappa(a+c)^2\right), \quad \forall n \geq 1. \end{aligned}$$

Using (5.50)-(5.52), we obtain

$$(5.53) \quad \begin{aligned} & J_{h,\kappa,\alpha}(q_n^h, p_n^h, q_n, p_n)(\theta) - \\ & -J_{h,\kappa,\alpha}(q_{\min,\kappa,\alpha}^h, p_{\min,\kappa,\alpha}^h, q_{\min,\kappa,\alpha}, p_{\min,\kappa,\alpha})(\theta) - \\ & -J'_{\kappa,\alpha}(q_{\min,\kappa,\alpha}, p_{\min,\kappa,\alpha})(\theta) (q_n - q_{\min,\kappa,\alpha}, p_n - p_{\min,\kappa,\alpha}) \geq \\ & \geq C_1 \exp\left(2\kappa(a-c)^2\right) \|(q_n - q_{\min,\kappa,\alpha}, p_n - p_{\min,\kappa,\alpha})\|_{H_{1,2,\theta}^2}^2 - \\ & -C_1 h \exp\left(2\kappa(a+c)^2\right), \quad \forall n \geq 1. \end{aligned}$$

Next, by (3.27)  $-J'_{\kappa,\alpha}(q_{\min,\kappa,\alpha}, p_{\min,\kappa,\alpha})(\theta) (q_n - q_{\min,\kappa,\alpha}, p_n - p_{\min,\kappa,\alpha}) \leq 0$ . Since  $-J_{h,\kappa,\alpha}(q_{\min,\kappa,\alpha}^h, p_{\min,\kappa,\alpha}^h, q_{\min,\kappa,\alpha}, p_{\min,\kappa,\alpha})(\theta) \leq 0$  as well, then (5.45) and (5.53) imply

$$(5.54) \quad \begin{aligned} & J_{h,\kappa,\alpha}(Z_n)(\theta) \geq \\ & \geq C_1 \exp\left(2\kappa(a-c)^2\right) \|(q_n - q_{\min,\kappa,\alpha}, p_n - p_{\min,\kappa,\alpha})\|_{H_{1,2,\theta}^2}^2 - \\ & -C_1 h \exp\left(2\kappa(a+c)^2\right), \quad \forall n \geq 1. \end{aligned}$$

Until now we have not used sufficiently large numbers  $n$ . We now start to use them. By (5.43), (5.44) and (5.46) there exists a sufficiently large integer  $N = N(h, \kappa, \alpha, \varepsilon, A, \theta) > 1$  depending only on listed parameters such that

$$J_{h,\kappa,\alpha}(Z_n)(\theta) \leq J_{h,\kappa,\alpha}(Z^*)(\theta), \quad \forall n \geq N, \quad \forall \theta \in [0, 2\pi].$$

Hence, (5.54) implies

$$(5.55) \quad \begin{aligned} & J_{h,\kappa,\alpha}(Z^*)(\theta) \geq \\ & \geq C_1 \exp\left(2\kappa(a-c)^2\right) \|(q_n - q_{\min,\kappa,\alpha}, p_n - p_{\min,\kappa,\alpha})\|_{H_{1,2,\theta}^2}^2 - \\ & -C_1 h \exp\left(2\kappa(a+c)^2\right), \quad \forall n \geq N. \end{aligned}$$

Using (3.44), Proposition 4.1, (4.10), (4.11), (4.23) and (5.46), we obtain

$$\begin{aligned}
& J_{h,\kappa,\alpha}(Z^*)(\theta) = J_{h,\kappa,\alpha}(q^{*h}, p^{*h}, q^*, p^*)(\theta) = \\
= & \sqrt{\varepsilon} \int_{\Omega,rt} \left[ (F_1^h(q^{*h}, p^{*h})(\mathbf{x}_{i,j}^h, \theta))^2 + (F_2^h(q^{*h}, p^{*h})(\mathbf{x}_{i,j}^h, \theta))^2 \right] W_\kappa^h(\mathbf{x}_{i,j}^h) d\mathbf{x}_{i,j}^h + \\
& + \alpha \|(q^*, p^*)\|_{H_{1,2,\theta}}^2 \leq \\
\leq & J_{\kappa,\alpha}(q^*, p^*) + C_1 h \exp\left(2\kappa(a+c)^2\right) \leq C_1 \alpha + C_1 h \exp\left(2\kappa(a+c)^2\right).
\end{aligned}$$

Combining this with (5.55), we obtain (5.47), which is the first target estimate of this theorem. The second target estimate (5.48) follows immediately from (3.39), (5.47) and triangle inequality. The third target estimate (5.49) follows immediately from (4.20)-(4.23) and (5.48).  $\square$

## 6. Deep Learning With A Priori Accuracy Estimates on the Training Stage.

**6.1. Estimating the accuracy of the starting point for the training step of deep learning.** We now estimate the accuracy of the starting point of iterations for the training step of our deep learning procedure. To simplify the presentation, we assume that conditions of Theorem 5.2 hold. The case of Theorem 5.3 is considered similarly.

Let  $\kappa_3$  and  $\theta_0$  be two numbers of Theorem 5.2. Since we now have only one value of the number  $\theta = \theta_0 \in [0, 2\pi]$  instead of the whole interval  $\theta \in [0, 2\pi]$ , then, recalling (3.9), (3.16), (3.28), (3.29) and using (5.28), we replace (3.30) with

$$(6.1) \quad r_{\kappa_3,\alpha}(\mathbf{x}_{i,j}^h) = -\left(\Delta^h \psi_{\min,\kappa_3,\alpha} + (\nabla \psi_{\min,\kappa_3,\alpha})^2\right)(\mathbf{x}_{i,j}^h, \theta_0).$$

Here the function  $r_{\kappa_3,\alpha}(\mathbf{x}_{i,j}^h)$  is our computational result obtained by the convexification method on a coarse grid. Next, we interpolate formula (6.1) on a fine grid in  $\Omega$  and apply the procedure described in (3.31)-(3.35). We obtain this way an approximation  $\sigma_{\kappa_3,\alpha}(\mathbf{x})$  of the true coefficient  $\sigma^*(\mathbf{x})$ . Because of this procedure, it is reasonable to assume that the accuracy of the latter approximation is the same as the one in (5.31), i.e.

$$(6.2) \quad \|\sigma_{\kappa_3,\alpha} - \sigma^*\|_{L_2(\Omega)} \leq C_1 \left(\sqrt{\alpha} + \sqrt{h}\right) \exp\left(\kappa_3(a+c)^2\right).$$

As it was pointed out in section 1, one of significantly new elements of this paper is that on the training step of deep learning we use the solution obtained by the semi-discrete version of the convexification method on a coarse grid as the starting point of iterations. In other words, we use the function  $\sigma_{\kappa_3,\alpha}(\mathbf{x})$  for this purpose. Therefore, (6.2) provides the desired accuracy estimate of the starting points for all cases of the training set of our deep learning procedure.

**6.2. Outline of the deep learning procedure for our case.** We propose an unsupervised hybrid image-to-image model that combines a Denoising Convolutional Neural Network (DnCNN) with a Residual U-Net enhanced by Squeeze-and-Excitation (SE) attention blocks. This architecture is designed for grayscale reconstruction tasks, such as denoising Chinese character images while preserving sharp strokes. For this image-to-image translation task, we adopt the U-Net architecture [32] (see Fig. 2), which has demonstrated remarkable success in biomedical image segmentation and other image restoration tasks. The U-Net consists of a contracting path (encoder) and an expansive path (decoder).

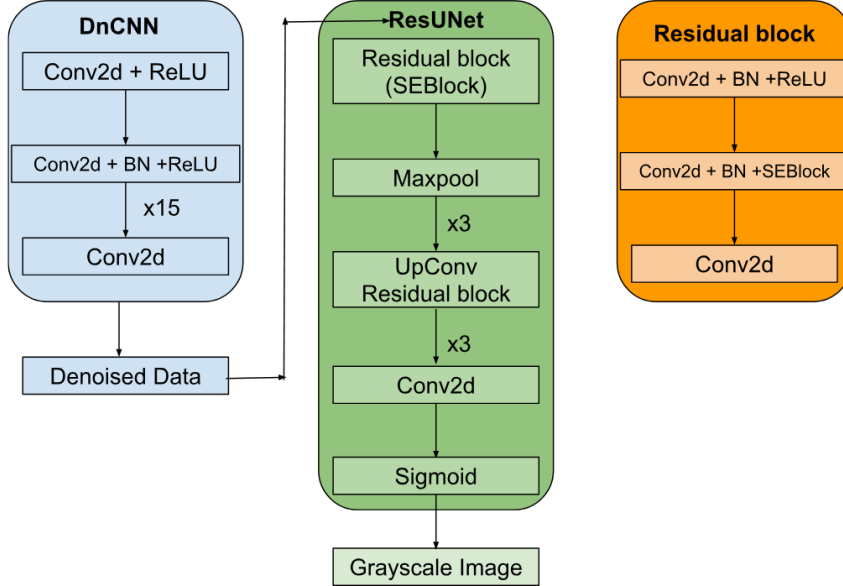


FIG. 2. Architecture of the proposed DnCNN + ResUNet model with SEBlock. The grayscale input image is denoised by DnCNN and then passed to a SE-enhanced ResUNet for reconstruction.

**6.3. Procedure.** The network is trained to minimize a loss function that measures the dissimilarity between its output  $\sigma_{pred}^{(i)} = \text{U-Net}(\sigma_{conv}^{(i)})$  and the true solution  $\sigma^{(i)*}$  for each  $i = 1, \dots, N$ . For each case number  $i = 1, \dots, N$  of training we use the above result obtained by the convexification method on the coarse grid, since it guarantees the accuracy estimate  $O(\sqrt{\alpha} + \sqrt{h})$  as  $\sqrt{\alpha} + \sqrt{h} \rightarrow 0$ .

To train the network, we require a large dataset of paired images

$$(\sigma_{conv}^{(i)}, \sigma^{(i)*}), \quad i = 1, \dots, N,$$

where  $\sigma^{(i)*}$  is the true solution for the case  $i$ , and  $\sigma_{conv}^{(i)}$  is the corresponding noisy reconstruction obtained from the semi-discrete convexification method on the coarse grid and interpolated then on a fine grid in  $\Omega$ , see subsection 6.1. The network is trained to minimize a loss function that measures the dissimilarity between its output  $\sigma_{pred} = \text{U-Net}(\sigma_{conv})$  [32] and the true solution  $\sigma^*$ . For each case number  $i = 1, \dots, N$  of training we use the above result obtained by the convexification method on the coarse grid, since it guarantees the accuracy estimate  $O(\sqrt{\alpha} + \sqrt{h})$  as  $\sqrt{\alpha} + \sqrt{h} \rightarrow 0$ . The network was trained using the loss function

$$(6.3) \quad \mathcal{L}_{total} = \gamma(1 - \text{MS-SSIM}) + (1 - \gamma) \text{L1Loss}, \quad \gamma = 0.84.$$

For each  $i = 1, \dots, N$  this function was minimized using  $\sigma_{conv}^{(i)}$  as the starting point of iterations.

**6.4. DnCNN denoising front-end.** The first stage is a 17-layer DnCNN:

- **Input:** Single-channel ( $1 \times 256 \times 256$ ) grayscale image.
- **Architecture:**
  - Initial layer: Conv2D( $1 \rightarrow 64$ , kernel = 3) + ReLU
  - 15 intermediate blocks: Conv2D( $64 \rightarrow 64$ , kernel = 3) + BatchNorm + ReLU
  - Final layer: Conv2D( $64 \rightarrow 1$ , kernel = 3)
- **Output:** Residual learning output,  $x - F(x)$ .

**6.5. ResUNet with SE self-attention.** The denoised image is passed to a Residual U-Net with SE attention blocks:

- **Encoder:**
  - 3 stages with downsampling via MaxPool2D(2)
  - Residual blocks with output channels:  $64 \rightarrow 128 \rightarrow 256$
  - Each residual block includes SE attention
- **Bottleneck:** One residual block with 512 channels
- **Decoder:**
  - 3 stages with ConvTranspose2D upsampling
  - Skip connections from encoder
  - Residual blocks with output channels:  $256 \rightarrow 128 \rightarrow 64$
- **Final Layer:** Conv2D( $64 \rightarrow 1$ ) + Sigmoid

**6.6. Squeeze-and-excitation (SE) block.** Each residual block is augmented with a channel-wise attention mechanism:

- Global average pooling across spatial dimensions
- Two-layer fully-connected network:

$$\text{FC}(C \rightarrow C/r \rightarrow C) + \text{Sigmoid}, \quad r = 16$$

- The output attention weights modulate the original feature maps channel-wise

**6.7. Loss function.** We adopt a combined loss of Multi-Scale Structural Similarity (MS-SSIM) and L1 loss (6.3). This loss function encourages both: perceptual fidelity and pixel-wise accuracy, especially for preserving the fine stroke structures in characters we image.

**6.8. Training details.**

- **Dataset:** Grayscale paired images (input: noisy reconstructions; label: corresponding clean ground-truth images).
- **Image resolution:** Both the noisy input reconstructions and the corresponding clean label images are represented on a  $256 \times 256$  pixel grid.
- **Dataset size and split:** The total number of cases was 3,256. Following the conventional practice for training/validation/testing splits, we use the 80%/10%/10% proportions [36]. Concretely, this corresponds to 2,604 cases for training, 326 for validation, and 326 for testing.
- **Optimizer:** AdamW (lr =  $10^{-3}$ , weight decay =  $10^{-5}$ ).
- **Scheduler:** ReduceLROnPlateau (factor 0.5, patience 3).
- **Epochs:** 200.
- **Batch size:** 4.
- **Framework:** PyTorch with CUDA acceleration.

**6.9. Evaluation metrics.** We evaluate the quality of the reconstruction using:

- **PSNR:** Peak Signal-to-Noise Ratio
- **Validation Loss:** MS-SSIM + L1 as described
- **Visual Inspection:** Qualitative comparison on held-out test images

The deep learning computations took 20 hours on an NVIDIA GeForce RTX 3080 Ti GPU.

**Training:** The model was trained for 200 epochs, with a total training time of approximately 20 hours. Throughout training, the RTX 3080 Ti consistently operated at near 100 % utilization while occupying almost the full available GPU memory, reflecting the memory-intensive nature of the network architecture and loss computation. In addition, CPU and system memory usage remained high, indicating efficient data handling and minimal hardware idle time. Overall, the training process effectively leveraged both GPU and CPU resources, demonstrating stable and efficient utilization of the available hardware despite the substantial computational load.

**6.10. Selection of the loss function (6.3).** We now explain the reason of the choice of the loss function in the form of (6.3), in which a combined MS-SSIM and L1 loss is used. MS-SSIM has assigned a higher weight to emphasize structural fidelity. This loss formulation proved effective for reconstructing Chinese characters, as MS-SSIM encourages multi-scale structural consistency, helping to preserve stroke continuity and global character geometry, while the L1 term enforces pixel-level accuracy and sharpness. The combination enables the model to suppress mosaic artifacts and coherently reconstruct missing or degraded regions, producing visually consistent characters that maintain both local detail and overall structural integrity.

### 6.11. Model summary table.

TABLE 1  
*Architecture Summary of Combined DnCNN + ResUNet Model.*

Component	Details
DnCNN	17-layer residual denoiser (Conv-BN-ReLU)
ResUNet	3-level encoder-decoder with skip connections
Residual Block	2 conv layers + SE attention + identity skip
SE Block	Channel-wise self-attention via squeeze and excitation
Loss	$\gamma = 0.84$ : MS-SSIM + L1
Output	Sigmoid to scale prediction to $[0, 1]$

**6.12. Numerical setup.** Our numerical setup for data generation via the solution of the forward problem and the semi-discrete convexification method is identical to the one used in [25]. We now briefly present it for the sake of completeness referring to [25] for some details.

For each  $\theta \in [0, 2\pi)$  and for the corresponding position  $\mathbf{x}_0 = \mathbf{x}_0(\theta) \in E_B(a, b)$  in (2.4) the forward problem (2.8) is solved by the Finite Element Method (FEM) in the disk  $P_D$  defined in (2.1). The radius of this disk is  $D = 3$  and its center is at the point  $(a, b) = (1.5, 1.5)$ , see Figure 1. The circle  $E_B(a, b)$  is now  $E_B(1.5, 1.5)$  with its radius  $B = 2$ . The spatial mesh size of the FEM is  $1/160$ . The square  $\Omega$  in (2.2) is now

$$(6.4) \quad \Omega = \{\mathbf{x} = (x, y) : 1 < x, y < 2\},$$

i.e.,  $c = 0.5$  in (2.2). The source function  $g(\mathbf{x} - \mathbf{x}_0)$  is as in (2.5) with  $\xi = 0.1$ . We use 199 discrete source positions corresponding to  $\theta_n = n\rho_\theta$ ,  $n = 1, 2, \dots, 199$ ,  $\rho_\theta = \pi/100$ .

For the convexification method we have used a finite difference scheme to discretize the Partial Differential Operators in (3.24) in the computational domain  $\Omega$  in (6.4). We have used a two coarse grids: with  $10 \times 10$  of  $20 \times 20$  pixels, which means grid step sizes  $h_1 = 0.1$  and  $h_2 = 0.05$  respectively in (4.1). On the other hand, the grid step size for the convexification method on the fine grid in [25, page 17] was  $h_3 = 1/40 = 0.025$ , i.e. two times less than  $h_2$ . This explains the  $14.25 = 57/4$  fold speed up in computations on the grid with  $h = h_2 = 0.05$ , see (1.1). We have used parameters  $\varepsilon, \kappa, \alpha$  in (3.24) the same as the ones in formula (8.6) of [25]:

$$\alpha = 0.01, \quad \varepsilon = 0.0002, \quad \kappa = 3.$$

Since the minimization in the convexification method is carried out on the set  $\overline{G_\theta(A)}$  with restrictions, see (3.22), then we have used the MATLAB built-in function **fminunc**. The true solutions and the output of the deep learning network are defined on a finer grid of  $128 \times 128$  pixels.

**7. Numerical Results.** Our test phantoms are based on Chinese characters, which provide a challenging test case due to their intricate shapes, sharp corners, and combination of thick and thin strokes. The conductivity is set to be  $\sigma = 2$  inside the character shape and  $\sigma = 1$  in the background. The images shown here are representative samples drawn from the testing set, evaluated after the training phase was completed.

We compare the reconstruction results obtained from two different spatial discretizations of the coarse grids:

1. A too coarse grid with step size

$$(7.1) \quad h_1 = 0.1.$$

2. A coarse grid with a finer grid with step size

$$(7.2) \quad h_2 = 0.05.$$

Images on Figures 3, 4 and 5 are obtained on the testing step of our deep learning procedure. Left columns show results of the performance of the semi-discrete version of the convexification method with two different grid step sizes (7.1) and (7.2). We point out that images in the left columns were not used on the testing step since the convexification method was used only to train the network. These two grid step sizes were used only on two versions of the training step.



FIG. 3. *Left column: image obtained by the semi-discrete version of the convexification method on a too coarse grid with the grid step size  $h_1 = 0.1$  as in (7.1). Right column: the true image. Middle column: the reconstructed image after deep learning. These results are visibly worse than those obtained with the a finer coarse grid step size  $h_2 = 0.05$  as in (7.2) in the next Figure 4. Apparently, the coarse grid step size  $h_1 = 0.1$  is too large.*

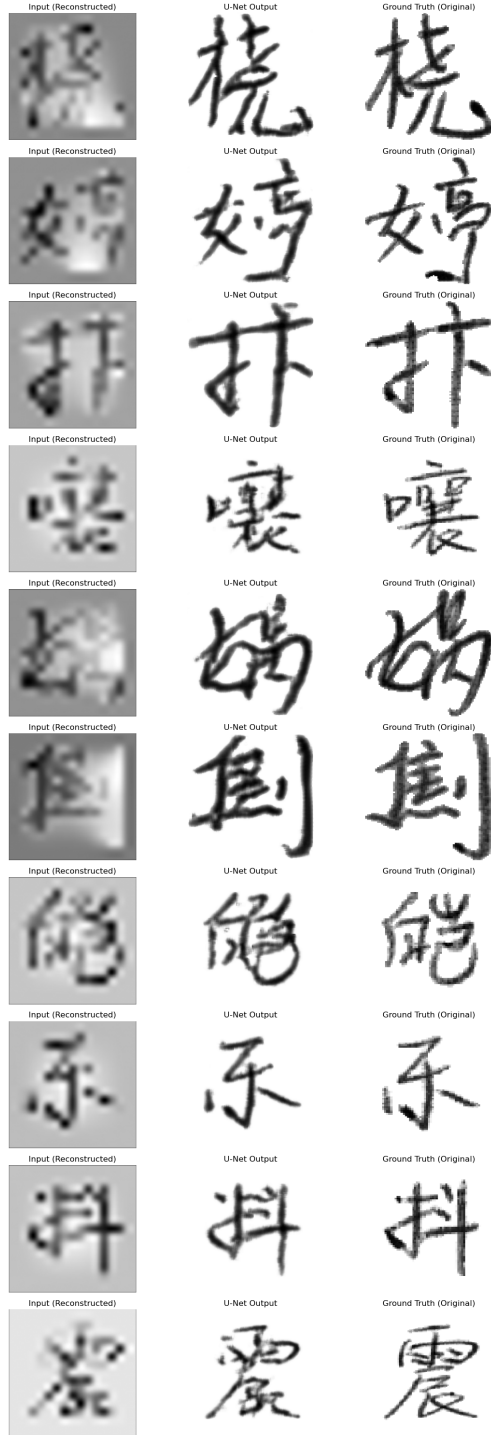


FIG. 4. Left column: the image obtained by the semi-discrete version of the convexification method on a coarse mesh with a finer coarse grid with step size  $h_2 = 0.05$  as in (7.2). The a priori accuracy estimate of the starting point is given in (6.2). Right column: the true image. The same characters are used in this column as in 3. Middle column: the reconstructed image after deep learning. One can observe an excellent reconstruction accuracy in the middle column. Our algorithm recovers quite well intricate structures and sharp contours.

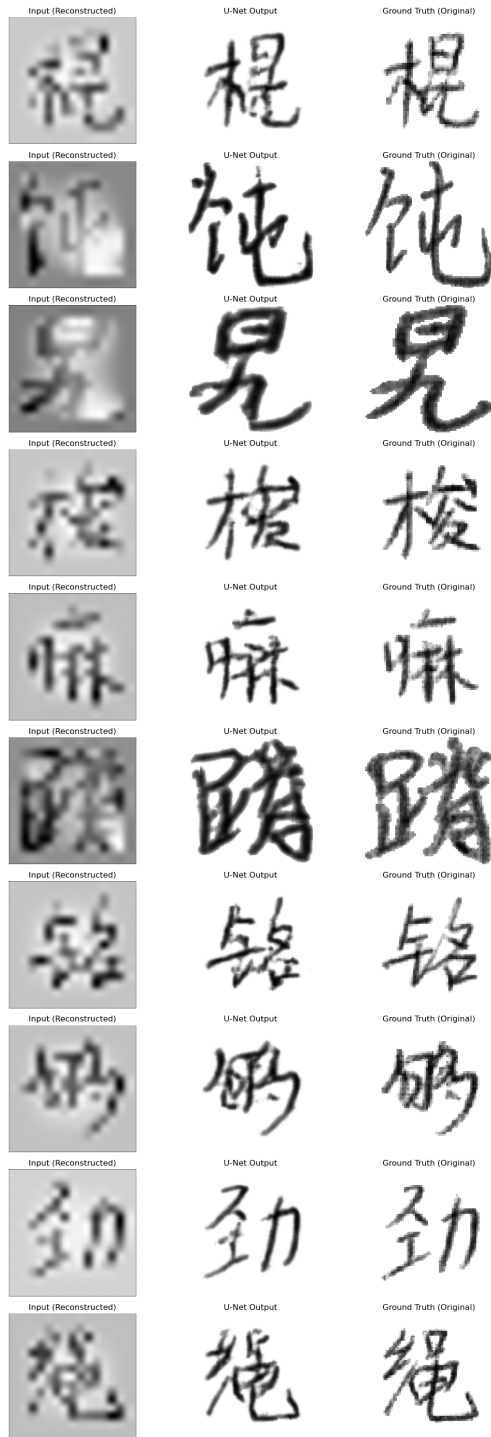


FIG. 5. This is the second series of images with the grid step size of a finer coarse grid  $h_2 = 0.05$  as in (7.2). Left column: image obtained by the semi-discrete version of the convexification method with  $h_2 = 0.05$ . Right column: the true image. Middle column: the reconstructed image after deep learning. The same high reconstruction accuracy as the one of Figure 4 is observed.

The same characters in the right column are used in Figures 3 and 4. This is done for the sake of comparisons of the results of our deep learning procedure for two different grid step sizes (7.1) and (7.2) of the convexification method on the training step. A clear qualitative difference can be observed between the results produced from the too coarse grid and the finer coarse grid of the semi-discrete version of the convexification method being applied on the training step. In the case (7.2) of a finer coarse grid, the output of our hybrid U-Net model closely resembles the ground truth Chinese characters. Most of the fundamental stroke structures such as horizontal strokes, vertical strokes, right-falling strokes, and left-falling strokes are well preserved. In particular, the network successfully identifies straight-line features as straight lines and reconstructs the relative orientation and placement of slanted strokes with reasonable accuracy. Moreover, the finer coarse grid result demonstrates a strong ability to distinguish between dots and short line segments, which is essential for the legibility of Chinese characters.

One can observe that the too coarse grid with  $h_1 = 0.1$  as in (7.1) produces outputs of Figure 3 that are largely illegible and fail to effectively resemble the original characters. Our hybrid U-Net model struggles to differentiate between vertical strokes and right-falling strokes, as well as between dots and line segments. This loss of structural distinction significantly degrades readability and makes character recognition nearly impossible in most cases.

In contrast to Figure 3, the primary limitation of the computational result of Figures 4 and 5 with  $h_2 = 0.05$  as in (7.2) appears in characters with highly crowded structures, especially those involving dense combinations of horizontal and vertical strokes forming square-like patterns. In these cases, the proximity of strokes reduces the available spatial resolution, making it more challenging for the network to accurately separate individual components. Nevertheless, aside from these tightly packed characters, the finer mesh consistently yields accurate and visually coherent reconstructions.

These observations highlight the critical role of the grid size and the initialization quality in our deep learning procedure. Since the performance of our hybrid U-Net model is inherently dependent on the information content of the training data, a finer discretization provides richer spatial features and more informative inputs. As a result, better initial conditions and stronger structural constraints lead to substantially improved learning outcomes and reconstruction accuracy.

**8. Conclusions.** We have proposed a new concept of the two-stage numerical procedure for Coefficient Inverse Problems. On the first stage a new semi-discrete version of the convexification numerical method is applied on a coarse grid. It is applied only on the training step of the deep learning procedure. The reason why the coarse grid is used is that the convexification performs slowly. On the second stage deep learning refines the images obtained on the first stage. A significantly new analytical element is a careful convergence analysis of that semi-discrete version since such an analysis was performed in for only continuous versions of the convexification method. Let  $h \in (0, 1)$  be the grid step size of the semi-discrete version of the convexification procedure. The notion of the  $h$ -strong convexity is introduced and actively explored for the first timeur convergence analysis ends up with an a priori accuracy estimate for the training set of the deep learning. Numerical experiments demonstrate both a high speed of computations and a high accuracy of reconstructions of complicated media structures.

**Acknowledgments:** The work of MVK was partially supported by the National

Science Foundation grant DMS 2436227. The authors are grateful to Dr. Jingzhi Li and Dr. Alexandre Timonov for useful discussions. Dr. Zhipeng Yang has computed the above described numerical results for the convexification method on sparse grids. He has obtained those results using the software, which he has developed for publication [25]. The authors are grateful to Dr. Yang for his kindness by providing those computational results for this publication.

## REFERENCES

- [1] L. Beilina, Domain decomposition finite element/finite difference method for the conductivity reconstruction in a hyperbolic equation, *Commun. Nonlinear Sci. Numer. Simul.* 37, 222–237, 2016.
- [2] L. Beilina and E. Lindström, An adaptive finite element/finite difference domain decomposition method for applications in microwave imaging, *Electronics*, 11, 1359, 2022.
- [3] L. Borcea. Electrical impedance tomography. *Inverse problems*, 18(6):R99, 2002.
- [4] A. L. Bukhgeim and M. V. Klibanov, Uniqueness in the large of a class of multidimensional inverse problems, *Soviet Math. Doklady*, 17 (1981), pp. 244–247.
- [5] G. Chavent. *Nonlinear Least Squares for Inverse Problems: Theoretical Foundations and Step-by-Step Guide for Applications*. Springer Science & Business Media, Berlin, 2010.
- [6] G. Giorgi, M. Brignone, R. Aramini, and M. Piana. Application of the inhomogeneous Lippmann–Schwinger equation to inverse scattering problems. *SIAM J. Appl. Math.*, 73:212–231, 2013.
- [7] A. V. Goncharsky and S. Y. Romanov. Iterative methods for solving coefficient inverse problems of wave tomography in models with attenuation. *Inverse Probl.*, 33:025003, 2017.
- [8] A. V. Goncharsky, S. Y. Romanov, and S. Y. Seryozhnikov. On mathematical problems of two-coefficient inverse problems of ultrasonic tomography. *Inverse Probl.*, 40:045026, 2024.
- [9] G. Gilbarg and N. S. Trudinger. *Elliptic Partial Differential Equations of Second Order*. Springer-Verlag, New York, second edition, 1983.
- [10] S. M. Goh, J. C. Ye, et al. Deep learning for EIT: a physics-informed approach. *Inverse Problems*, 35(10):105008, 2019.
- [11] B. Harrah, The Calderon problem with finitely many unknowns is equivalent to convex semi definite optimization, *SIAM J. Math. Anal.*, 55, 5666–5684, 2023.
- [12] B. Harrah and H. Meftahi, A monotonicity-based globalization of the level-set method for inclusion detection, *Commun. Anal. Comput.* 5, 1–17, 2025.
- [13] B. Harrah and A. Brojatsch, On the required number of electrodes for uniqueness and convex reformulation in an inverse coefficient problem, *Inverse Problems*, 41: 105011, 2025.
- [14] V. Isakov, *Inverse Problems for Partial Differential Equations*. Springer, New York, 2006.
- [15] M.V. Klibanov and O.V. Ioussoupova, Uniform strict convexity of a cost functional for three dimensional inverse scattering problem, *SIAM J. Mathematical Analysis*, 26, 147-179, 1995.
- [16] M. V. Klibanov. Global convexity in a three-dimensional inverse acoustic problem. *SIAM J. Math. Anal.*, 28:1371–1388, 1997.
- [17] M. V. Klibanov and A. Timonov, *Carleman Estimates for Coefficient Inverse Problems and Numerical Applications*, VSP, Utrecht, 2004.
- [18] M. V. Klibanov, J. Li, and W. Zhang. Electrical impedance tomography with restricted Dirichlet-to-Neumann map data. *Inverse Probl.*, 35:035005, 2019.
- [19] M. V. Klibanov and J. Li, *Inverse Problems and Carleman Estimates: Global Uniqueness, Global Convergence and Experimental Data*. De Gruyter, Berlin, 2021.
- [20] M. V. Klibanov, L. H. Nguyen, and H. V. Tran. Numerical viscosity solutions to Hamilton-Jacobi equations via a Carleman estimate and the convexification method. *Journal of Computational Physics*, 451:110828, 2022.
- [21] M.V. Klibanov, J. Li and W. Zhang, A globally convergent numerical method for a 3D coefficient inverse problem for a wave-like equation, *SIAM J. Scientific Computing*, 44, A3341–A3365, 2022.
- [22] M.V. Klibanov, A.A. Shananin, K.V. Golubnichiy and S.M. Kravchenko, Forecasting stock options prices via the solution of an ill-posed problem for the Black–Scholes equation, *Inverse Problems*, 38, 115008, 2022.
- [23] M. V. Klibanov, J. Li, and Z. Yang, Convexification for the viscosity solution for a coefficient inverse problem for the radiative transport equation, 39, 125002, 2023.
- [24] M. V. Klibanov, K.V. Golubnichiy and A.V. Nikitin, Quasi-reversibility method and neural network machine learning for forecasting of stock option prices, *Contemporary Mathematics*,

- 784, 129-144, 2023.
- [25] M. V. Klibanov, J. Li, and Z. Yang. Convexification with the viscosity term for electrical impedance tomography. *Inverse Problems*, 41, 065020, 2025.
  - [26] M. V. Klibanov and A. Timonov, Acoustic imaging via a viscosity approximation of an elliptic system generated by the Lavrent'ev integral operator, *SIAM J. Imaging Sciences*, 18, 1002–1027, 2025.
  - [27] M.V. Klibanov, J. Li, V.G. Romanov and Z. Yang, Convexification for the 3D problem of travel time tomography, *SIAM J. Scientific Computing*, 47, A1436-A1457, 2025.
  - [28] M.M. Lavrent'ev, V.G. Romanov and S.P. Shishatskii, *Ill-Posed Problems of Mathematical Physics and Analysis*, AMS, Providence: RI, 1986.
  - [29] H.P.N. Le, T. T. Le, and L. H. Nguyen. The Carleman convexification method for Hamilton-Jacobi equations. *Computers & Mathematics with Applications*, 159, 173–185, 2024.
  - [30] R.G. Novikov, The  $\bar{\partial}$ - approach to approximate inverse scattering at fixed energy in three dimensions, *International Math. Research Reports*, 6 (2005), 287-349.
  - [31] V.G. Romanov, *Investigation Methods for Inverse Problems*, VSP, Utrecht, The Netherlands, 2002.
  - [32] O. Ronneberger, P. Fischer and T. Brox. U-net: Convolutional networks for biomedical image segmentation. In *International Conference on Medical image computing and computer-assisted intervention*, pages 234–241, Springer, 2015.
  - [33] T.B.R. Santos, R.M. Nakanishi, T.M.M. Olegário, R.G. Lima and J.L. Mueller, Resolution improvement and algorithmic dependence of machine learning for post-processing respiratory EIT images, *Applied Mathematics for Modern Challenges*, 1, 21-38, 2023.
  - [34] J.A. Scales, M.L. Smith and T.L. Fisher, Global optimization methods for multimodal inverse problems, *J. Comput. Phys.*, 103, 258-268, 1992.
  - [35] A.N. Tikhonov, A.V. Goncharsky, V.V. Stepanov and A.G. Yagola, *Numerical Methods for the Solution of Ill-Posed Problems*, Kluwer, London, 1995.
  - [36] C. Lokker, E. Bagheri, W. Abdelkader, R. Parrish, M. Afzal, T. Navarro, C. Cotoi, F. Germini, L. Linkins, R. B. Haynes, L. Chu and A. Iorio, Deep learning to refine the identification of high-quality clinical research articles from the biomedical literature: Performance evaluation, *J. Biomed. Inform.* 142, 104384, 2023.